Energy Conversion and Management 244 (2021) 114469

Contents lists available at ScienceDirect

Energy Conversion and Management

journal homepage: www.elsevier.com/locate/enconman

A layout optimization method based on wave wake preprocessing concept for wave-wind hybrid energy farms

Francisco Haces-Fernandez [a], Hua Li [b,*], David Ramirez [c]

[a] Department of Management, Marketing and Information Systems, Texas A&M University-Kingsville, Kingsville, TX 78363, USA
[b] Department of Mechanical and Industrial Engineering, Texas A&M University-Kingsville, Kingsville, TX 78363, USA
[c] Department of Environmental Engineering, Texas A&M University-Kingsville, Kingsville, TX 78363, USA

ARTICLE INFO

Keywords:
Wave wake preprocessing
Layout optimization
Wind wake
Genetic algorithm
Hybrid energy farm

ABSTRACT

Major investment of renewable energy currently focuses on wind and solar, which are commercially mature. However, there is no large commercial application of wave energy, despite more than four decades of continuous development. Previous research has indicated that wave energy could supply a significant portion of world electricity consumption. Therefore, it is critical to incentivize the utilization of wave energy. The hybrid energy farms, combining wave energy with wind energy, have been considered as one of the most viable solutions to promote mature grid integration of wave energy. However, combining wind and wave requires the identification of adequate locations for both resources and development of layout optimization algorithms capable of handling the complexity of wave wakes. Wave wake analysis has been one of the biggest hurdles for the development of recursive wave farm layout optimization algorithms due to the required extremely time consuming computation processes for each wave wake iteration. This research proposes a new approach by preprocessing the wave wakes beforehand the actual execution of the recursive layout optimization algorithm. This proposed preprocessed wave wake model can be integrated with the different optimization algorithms to identify optimal layouts for hybrid wave-wind farms. The new approach was tested in two selected locations in the Gulf of Mexico with over 36 years (1979–2015) of historical meteorological data. It identifies locations capable of sustaining commercially viable levels of wind and wave energy while simultaneously avoiding risk from extreme oceanic conditions that in the past have damaged or destroyed wave energy converters. Although the two locations have different meteorological conditions, the new approach was able to identify layouts with promising results in both locations. Results indicated that the selected locations could produce very good power output with a wave-wind hybrid energy farm, and most wave and wind energy devices generated capacity factor with values higher than commercial threshold limits.

1. Introduction

Wave energy is one of the most concentrated and persistent renewable energy resources [1]. It has the second highest theoretical energy potential among all ocean renewable energy sources, even higher than offshore wind energy [2]. The possibility of generating electricity extracting wave energy to supply both coastal [3]and offshore activities has been researched with great interests for more than four decades [4]. Wave energy has the potential to provide one third of United States (US) electricity consumption [5]. Considering that half of the population of the United States live within 50 miles of the coast, wave energy could significantly aid in decarbonizing the economy [6]. Additionally, offshore industrial activities, such as oil and gas platforms, could be supplied from wave energy, reducing operating costs and pollution [7]. Furthermore, wave energy applications are being developed by the US Navy for missions in high seas [8].

However, despite significant public and private interests in this topic, there is no large scale commercial wave energy converters (WECs) in operation [9]. A large number of designs and prototypes have been developed and tested [10], but no design standard has been widely adopted [6]. One of the main challenges for wave energy harvesting is its high variability [11], partially due to its dependence to two meteorological factors: wave height and wave period [12]. Other renewable energy resources, which are commercially mature, such as wind and

* Corresponding author.
E-mail addresses: Francisco.HacesFernandez@tamuk.edu (F. Haces-Fernandez), hua.li@tamuk.edu (H. Li), david.ramirez@tamuk.edu (D. Ramirez).

https://doi.org/10.1016/j.enconman.2021.114469
Received 26 January 2021; Accepted 25 June 2021

solar, are only dependent on one meteorological factor, wind speed and solar radiation, respectively. This makes their characterization less challenging than wave energy, which provides better opportunities to create and optimize successful harvesting equipment. Collocating WECs with other renewable energy devices dependent on just one factor, such as wind, would increase the potential of wave energy's commercial utilization [13].

Substantial additional public and private investments are required to bring wave energy from research and development (R&D) to commercial application [14]. However, more emphasis has been devoted to continue developing successful renewable energy technologies such as wind and solar [6]. The lack of investment on the wave energy sector has been exacerbated by past unsuccessful wave energy ventures [15], where diverse designs were underperformed, damaged, or destroyed [16] under extreme oceanic conditions [17]. It is estimated that a wave energy project has a failure risk of 75–90% in a twenty years lifespan project [13]. Extreme environmental conditions causing WEC failures are in many cases unforeseen [18] due to the diverse wave characteristics and variability in different locations [12]. Although it is well known that waves are generated from the transfer of energy from wind systems to the oceans [1], the cycle of creation, transport, evolution and disappearance of wave energy is different with the cycle of wave, and varies at different locations. Wave energy generation depends on local geographical and meteorological conditions [19]. Enclosed oceans, such as the Mediterranean [20]and the Caspian Sea [21], have high dependency of local weather patterns for the generation of wave energy due to fewer and smaller swells [1]. On the other hand, large oceanic areas, such as the Pacific ocean, create waves on remote locations where large wind systems interact with the ocean, developing some of the most energetic waves [22]. These waves, which are mostly independent from their originating wind systems, are able to travel long distance on wave trains as swells to reach distant areas such as the US West Coast [23]. Waves generated in these large oceanic areas are able to reach higher energetic levels and cause damages to WECs. On the other hand, some oceanic areas, such as the Gulf of Mexico (GoM), are semi enclosed locations, where most of the waves are generated by local wind systems with certain percentage of wave generated by swells from the Caribbean and the Atlantic Oceans [23]. These waves have significant energy levels without reaching the extreme values of open ocean waves. In this context, developing wave energy in the GoM, as a semi enclosed location, would reduce the risk of damage to the equipment, allow adequate wave energy harvesting and improve the success rate of wave energy project.

Wave-wind hybrid projects have been considered as a practical solution to accelerate wave energy development, incentivizing private and public investment in different projects [24]. Studies have shown that combining wave energy with wind energy could generate many synergetic benefits [25]. These benefits include significantly reducing power output variability [22], improving harvesting logistic [7]and integration to the grid [26], lowering costs [13], and providing higher reliability [27]. The GoM has been previously studied to evaluate the advantages of combining wave and wind resources, and the results have indicated that a significant variability reduction could be obtained [23] coupled with area usage maximization [22] and operation and maintenance cost reductions [27].

However, previous research has faced challenges when incorporating wave wake analysis in recursive optimization algorithms for hybrid wave-wind energy farms due to its intense use of computational resources and time consuming process for each iteration, making the entire optimization process super slow and impractical to get optimal results [28]. This research provides a novel approach to incorporate wave wakes in recursive optimization algorithms through preprocessing. Wave wakes are evaluated in advance of the execution of the optimization algorithm, and results are stored in a computer file to be used as posteriori by the recursive algorithm. It generates high savings in time and computational resources, making the layout algorithm for hybrid wave-wind farms feasible and pratical. This novel approach allows the proposed algorithm to be executed in conventional computer resources, without requiring high performance computing resources. In this paper, the wave wake preprocessing concept was integrated with an optimization algorithm to create a layout optimization method to identify the best layout of wave and wind hybrid energy farms, in which wave energy was selected as major energy source and wind energy was considered as secondary energy source. The new approach enables the optimization method to use local meteorological conditions to calculate wave and wind power output for diverse layouts and optimize the layouts to maximize the power output considering the wind and wave wakes caused by the devices under each particular meteorological condition.

The developed layout optimization method was further modified to ensure the wave energy was the major energy source in the energy farm since the original purpose of this research was to promote wave energy harvesting by reducing its power output variability through introducing wind energy as secondary energy source. Data from the WaveWatch III system developed by the National Oceanic and Atmospheric Administration (NOAA) was used along with a geographic information system (GIS) method. The detailed method is described in the following section. The GoM was chosen as the studying area, in which two specific locations in the GoM were selected as case studies to validate the new optimization method. The results are presented and discussed in the third section, which clearly show the effectiveness of the new optimization method.

2. Methods

Wave wakes have been studied for a long time because of its effects on marine navigation and offshore structures. Lord Kelvin in the 1880′s developed a model for the wake caused by ships and it has been studied extensively [29] through mathematical modelling [30] and geometric constructs [31]. As offshore oil and gas platforms started to be installed in deeper offshore areas, mathematical models were developed to evaluate the impact of waves and its wakes on these structures [32]. These models have been applied by previous research on WEC wake modelling [33]. However, these models required extensive computational calculations [34] and numerical analysis [35] even when calculating the wake of a single object [36]. The complexity increases when wakes are evaluated through three dimensional computational fluid dynamics (CFD) models [37] or remote sensing [38]. Therefore, these previous models are not appropriate for practical applications in hybrid energy farm layout optimization algorithms. In this research, a new method was developed to preprocess wave wake analysis after identifying the potential locations, which can be used together with genetic algorithm or other optimization algorithms without requiring extensive computational resources and capacity.

2.1. Wave wake model

In this paper, the Penney and Price wave wake model [39] was chosen to calculate the wave wakes generated by the WECs and the foundations of offshore wind turbines (OWTs). The selected model has been used by previous research on wave energy, including in the evaluation of permeable breakwaters by Hotta [40] and assessment of WECs by Monk et al. [41]. In these cases, it has shown good fitness with wave wake results, represented by the model [42]. The reduction in wave height caused by a fully reflecting breakwater was described by Penney and Price as a diffraction coefficient (K_d). The diffraction coefficient (K_d) is defined as the ratio between the reduced wave height ($H_{x,y}$) at any given location (x, y) downstream from the obstacle and the wave height of the original undisturbed wave (H_0) as Eq. (1) indicates [41]. As shown in Eq. (1), K_d is directly related to the coordinates (x, y), which can be converted to polar coordinate system as shown in Fig. 1. The presented mathematical model allows K_d to be higher than one, indicating wave

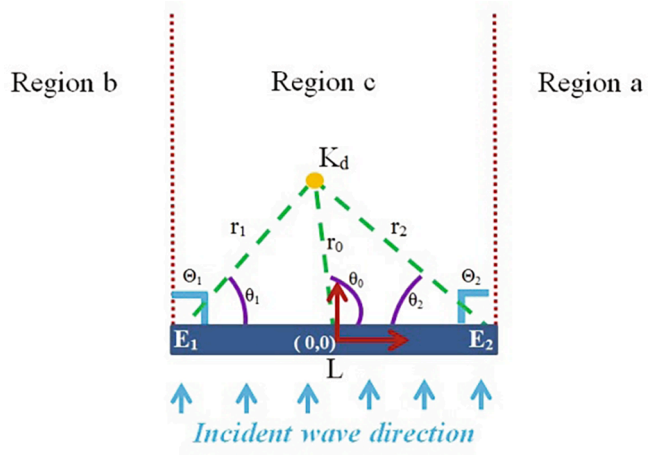

Fig. 1. Illustration of different factors involved in calculating K_d with only one obstacle using Penney and Price wave wake model.

energy enhancement due to the obstacle in particular locations.

$$K_d = \frac{H_{x,y}}{H_0} = |F(x,y)| = F(r,\theta) \tag{1}$$

As indicated in Fig. 1, when calculating K_d of the wave wake generated by only one WEC or one OWT foundation, the central point of the obstacle was assumed as origin of the coordinate system. After converting it to polar coordinate system, the distances from the given location to the origin, left and right ends of the obstacle were represented as r_0, r_1, and r_2, respectively. The angel between r_0 and x-axis was represented as θ_0. The angles between the obstacle and the lines of the given location to both ends were represented as θ_1 and θ_2. The length of the obstacle was represented by L. For the WEC that can be approximated as a series of heaving buoys due to its two degrees of freedom movement [43], L equals 13.6 m [44] considering its capture width [45]. For the OWTs, wave scattering was considered with L equaling 5 m as a jacket offshore foundation. Since the Pelamis is able to adjust their orientation while OWT foundation is normally cylindrical with the same face profile to the incident waves, both the WEC and OWT were considered to be perpendicular to the incident wave direction [46], so the angle between the obstacle and incident wave (Θ_0) and the angels between the two ends of the obstacle and incident waves (Θ_1 and Θ_2) were always 90° in this paper [47]. Meanwhile, the entire area after the obstacle was divided into three regions (a, b, and c) as indicated in Fig. 1. The length of a Pelamis WEC is considered as perpendicular to the incident waves while its width is evaluated as parallel to the wave direction. The parameter L for this analysis, as previously indicated, is consistent with Pelamis's capture width.

When the wave wake was only caused by one obstacle (either WEC or OWT's foundation), the complex approximate functions as indicated in Eq. (2), which were derived from Penney and Price wake model [39], were used in this paper to estimate K_d in different regions as function of r and θ in polar coordinate system [41].

In Eq. (2), the reflection coefficient (c_ρ) indicates total wave reflection when it equals to one and total wave absorption when it equals to zero. The transmission coefficient (c_l) indicates full transmission when it equals to one and no transmission when it equals to zero. In this research, c_ρ was set as 0.3 and c_l was set as 0.5 [33,41]. The incident planar wave component (I) and the reflective planar component (R) were calculated using Eqs. (3) and (4), respectively. It should be noted that the subscript j used in the following equations equals 0, 1, or 2. In general, the phase shift $\varepsilon_B$was calculated using Eq. (5). Since Θ_0 was assumed to be 90°, $\varepsilon_B$equals to zero.

$$I_j = cos\left[k^*r_j^*cos\left(\left(\theta_j - \Theta_j\right) + \varepsilon_B\right)\right] - isin\left[k^*r_j^*cos\left(\left(\theta_j - \Theta_j\right) + \varepsilon_B\right)\right] \tag{3}$$

$$R_j = cos\left[k^*r_j^*cos\left(\left(\theta_j + \Theta_j\right) + \varepsilon_B\right)\right] - isin\left[k^*r_j^*cos\left(\left(\theta_j + \Theta_j\right) + \varepsilon_B\right)\right] \tag{4}$$

$$\varepsilon_B = \pm k(L/2)\cos(\Theta_0) \tag{5}$$

The wave number k is related to the wave period T according to the dispersion relationship indicated by Eq. (6), where h is the depth of the water, g is the gravity, and ω is the angular frequency given by $\omega = 2\pi/T$.

$$\omega^2 = (2\frac{\pi}{T})^2 = g^*k^*tanh(k^*h) \tag{6}$$

The function $f(\sigma)$ is represented by Eq. (7) [41], and $f(\sigma^{'})$ can be represented by replacing σ with $\sigma^{'}$ in Eq. (7).

$$\begin{aligned}\int(\sigma_j) = 1 - \int(-\sigma_j) &= \frac{1+i}{2}\int_2^{\sigma_j} e^{\frac{\pi^*i^*u^2}{2}}du \\ &= \frac{1}{2}^*\left[\left(1 + C(\sigma_j) + S(\sigma_j) - i\left(S(\sigma_j) - C(\sigma_j)\right)\right)\right]\end{aligned} \tag{7}$$

The upper limit (σ or $\sigma^{'}$) of the integral in Eq. (7) was calculated using Eq. (8) or (9) according to the Penney and Price wake model since wake effect caused by reflected wave was not considered in this paper.

$$\sigma_j = 2\sqrt{\frac{kr_j}{\pi}sin\frac{1}{2}(\theta_j - \Theta_j)} \tag{8}$$

$$\sigma_j^{'} = -2\sqrt{\frac{kr_j}{\pi}sin\frac{1}{2}(\theta_j + \Theta_j)} \tag{9}$$

The terms $C(\sigma)$ and $S(\sigma)$ (or $C(\sigma^{'})$ and $S(\sigma^{'})$) in Eq. (7) are the Fresnel Integrals that can be calculated using Eqs. (10) and (11) applying the polynomial approximations proposed by McCormick and Kramer [48], which have indicated very good accuracy while significantly reducing the computational expenditure [41]. In both Eqs. (10) and (11), (σ_j) was considered as 0.002 as maximum error value since $\varepsilon(\sigma_j)\leqslant 0.002$.

$$\begin{aligned}C(\sigma_j) &= -C(-\sigma_j) \\ &\approx \frac{1}{2} + \frac{(1+0.926\sigma_j)sin\left(\frac{\pi\sigma_j^2}{2}\right)}{2+1.792\sigma_j+3.103\sigma_j^2} - \frac{cos\left(\frac{\sigma_j^2}{2}\right)}{2+4.142\sigma_j+3.492\sigma_j^2+6.670\sigma_j^3} + \int(\sigma_j)\end{aligned} \tag{10}$$

$$F(r,\theta) = \begin{cases} f(-\sigma_1)I_1 + c_\rho f\left(-\sigma_1^{'}\right)R_1 + f(\sigma_2)I_2 + c_\rho f\left(-\sigma_2^{'}\right)R_2 + c_l(f(\sigma_1)I_1 + f(-\sigma_2)I_2 - I_0), & region\ a \\ f(\sigma_1)I_1 + c_\rho f\left(-\sigma_1^{'}\right)R_1 + f(-\sigma_2)I_2 + c_\rho f\left(-\sigma_2^{'}\right)R_2 + c_l(f(-\sigma_1)I_1 + f(\sigma_2)I_2 - I_0), & region\ b \\ f(-\sigma_1)I_1 + c_\rho f\left(-\sigma_1^{'}\right)R_1 + f(-\sigma_2)I_2 + c_\rho f\left(-\sigma_2^{'}\right)R_2 + c_l(f(\sigma_1)I_1 + f(\sigma_2)I_2 - I_0), & region\ c \end{cases} \tag{2}$$

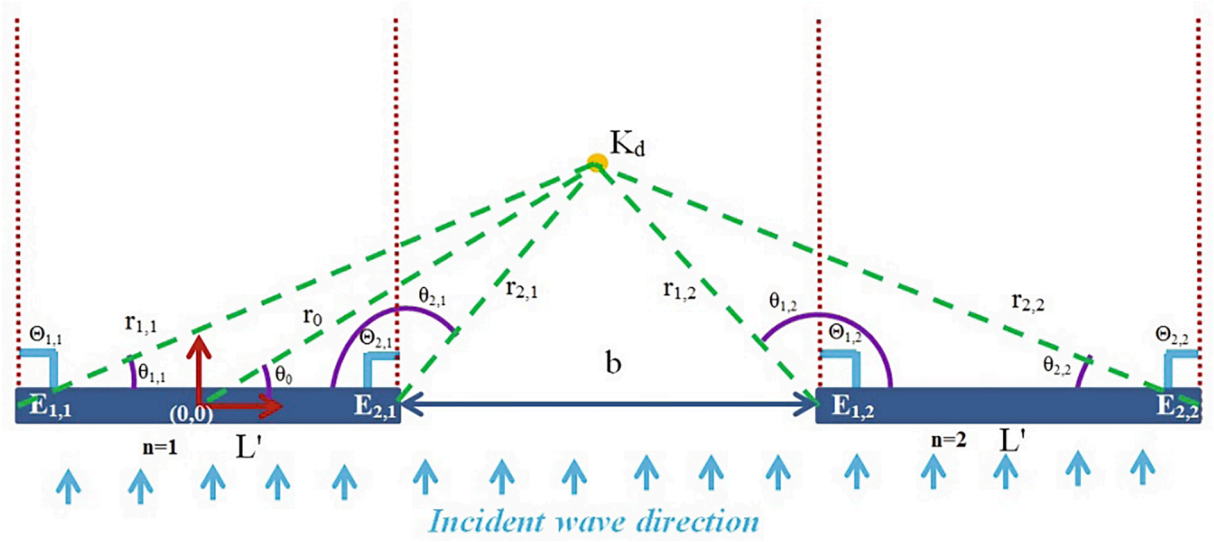

Fig. 2. Illustration of different factors involved in calculating K_d with two obstacles using Penney and Price wave wake model.

$$S(\sigma_j) = -S(-\sigma_j)$$
$$\approx \frac{1}{2} + \frac{(1+0.926\sigma_j)cos\left(\frac{\pi\sigma_j^2}{2}\right)}{2+1.792\sigma_j+3.103\sigma_j^2} - \frac{sin\left(\frac{\sigma_j^2}{2}\right)}{2+4.142\sigma_j+3.492\sigma_j^2+6.670\sigma_j^3} + \int(\sigma_j) \quad (11)$$

When a given location was affected by two wave wakes generated from two different obstacles (as shown in Fig. 2), Eq. (2) was no longer able to calculate the K_d of the given location. To calculate the K_d value due to wave wakes interactions, the approximate solution proposed by Hotta [40] and applied by Monk et al. to WECs [41] was considered in this paper. If the two obstacles have same length, the L' equals the obstacle's length. If the two obstacles have different length (one WEC and one OWT's foundation), the L' equals the average of the two obstacles' lengths. As discussed above, the angel between the obstacle and incident wave (Θ_0) and the angels between the two ends of the obstacle and incident waves ($\Theta_{1,n}$ and $\Theta_{2,n}$) were always 90° in this paper.

To calculate the K_d value, a temporary solution as defined by Eq. (12) was applied by considering only one obstacle at a time [41], where m = 1 or 2, and n = 1 or 2.

$$\tau_n(r_{m,n}, \theta_{m,n}) = F_n(r_{m,n}, \theta_{m,n}) - I_0 \quad (12)$$

$F_n(r_{m,n}, \theta_{m,n})$ in Eq. (12) was still calculated using Eq. (2), however, the given location would be located in different regions when considering different obstacles (n = 1 or 2). For example, the given location in Fig. 2 is in region of the left obstacle (n = 1), while it is in region c of the right obstacle (n = 2). In addition, the incident planar wave component (I) and the reflective planar component (R) were calculated using Eqs. (13), (14) and (15) instead of Eqs. (3) and (4) when considering two obstacles. Since $\Theta_{0,n}$ is assumed to be 90°, the obstacle phase shifts ε_B and μ_n equal to zero.

$$I_0 = \cos[k^* r_0 cos(\theta_0\text{-}\Theta_0) + \varepsilon_B + \mu_n] - i\sin[k^* r_0 \cos(\theta_0\text{-}\Theta_0) + \varepsilon_B + \mu_n] \quad (13)$$

$$I_{m,n} = \cos\left[k^* r_{m,n} cos(\theta_{m,n}\text{-}\Theta_{m,n}) + \varepsilon_B + \mu_n\right] - i\sin\left[k^* r_{m,n} \cos(\theta_{m,n}\text{-}\Theta_{m,n}) + \varepsilon_B + \mu_n\right] \quad (14)$$

$$R_{m,n} = \cos\left[k^* r_{m,n} cos(\theta_{m,n} + \Theta_{m,n}) + \varepsilon_B + \mu_n\right] - i\sin\left[k^* r_{m,n} \cos(\theta_{m,n} + \Theta_{m,n}) + \varepsilon_B + \mu_n\right] \quad (15)$$

$$\mu_n = \pm k(b + L^{'}) cos(\Theta_0) \quad (16)$$

Combining the two temporary solutions, the K_d value caused by wave wakes from two obstacles could be estimated using Eq. (17).

$$F(r,\theta)_{combined} = I_0 + \sum_{n=1}^{2} \tau_n(r,\theta) \quad (17)$$

The front row of WECs generated K_d values between 0.85 and 0.95 for single obstacle and two obstacles, respectively, while the WECs after first row generated K_d values between 0.40 and 0.60, which matched with results in previous literatures [41,49].

2.2. Wind wake model

The Jensen wind wake model was used in this paper to evaluate the wind wakes generated by OWT blades. The model was originally developed by Jensen [50] and improved by Frandsen [51] and Katic [52]. It has been used and validated by diverse previous studies [51], accurately predicting wind farm losses due to wake interference [53]. The model has been successfully applied for layout optimization using genetic algorithm [54] and with wind turbines at different heights [55]. The Jensen wind wake model is used by most studies for wind farms, showing accuracy for both onshore and offshore wind farms [56]. Wind energy developers have used the model to evaluate wind power output [57] applying diverse wind turbine models [58].

In the Jensen wind wake model, the wind wake is considered to create a volumetric expansion right after the rotor and to propagate continually and linearly as a wake behind the wind turbine, reducing the wind speed available for downstream turbines [59]. According to previous research [55], Eq. (18) computes the wind speed (U_i) available to wind turbine i considering the freestream wind speed (U_0) in m/s [51]. In this context, the rotor area of wind turbine i (A) is measured in m^2, while the $A_{overlap}$ (m^2) is the overlap area between rotor area of wind turbine i and the wake area generated from upstream wind turbines. $A_{overlap}$ is calculated as the intersecting areas of the turbulent wake's discs through geometric analysis applying the cosines law [55], while the radius of wake (r_1) at wind turbine i is estimated using Eq. (19). U_{def} is wind speed deficit, which is calculated using Eq. (20) with the axial induction factor (a), the entrainment constant (α), the adjusted rotor radius of wind turbine i (r_r in meters), and the distance between wind turbine i to the upstream wind turbine causing the wake (x in meters).

$$U_i = U_0{}^*\left[1 - U_{def}\left(A_{overlap}/A\right)\right] \quad (18)$$

$$r_1 = \alpha x + r_r \tag{19}$$

$$U_{def} = \frac{2a}{\left(1 + \alpha \frac{x}{r_r}\right)^2} \tag{20}$$

The axial induction factor (a) is calculated using Eq. (21), in which the thrust coefficient (C_T) was considered as 0.88 in concordance with previous research [55]. The adjusted rotor radius of wind turbine i (r_r) is calculated using Eq. (22), where r is the original rotor radius of wind turbine i [60].

$$C_T = 4a(1 - a) \tag{21}$$

$$r_r = r\sqrt{(1 - 0.5(a))/(1 - a)} \tag{22}$$

The entrainment constant (α) is calculated using Eq. (23), in which the surface roughness length (Z_0) was considered as 0.0002 (water surface) as indicated by empirical values and Z_i represents the hub height (meters) of wind turbine i.

$$\alpha = \frac{0.5}{ln(Z_i/Z_0)} \tag{23}$$

2.3. Selection of energy devices

To conduct layout optimization for a given wave-wind hybrid energy farm, WECs and OWTs need to be selected first. In this paper, the Pelamis P2 750 kW WEC and the Vestas V90 3 MW OWT were selected. Although there are no large scale commercial wave energy farms in operation, the Pelamis P1 750 kW was the first WEC to be connected to the grid in Aguçadoura, Portugal [61]. The project was shut down due to the financial issues of the owner Babcock & Brown in the 2008 financial crisis. The Pelamis P2 750 kW WEC, with improvement based on the Pelamis P1, was tested for more than three years in the Scottish test site of Billia Croo with excellent results [61,62]. The Pelamis P2 750 kW WEC was considered one of the most promising WECs for commercialization. It has been used extensively by previous research on wave energy [63] and compares very favorably with other WECs [21]. Its power table was released by its developer as illustrated in Fig. 3, which is easy to be used with WaveWatch III data to estimate the power output. Since Pelamis P2 750 kW WEC changes its orientation according to the incident wave and aligns itself as same as the direction of incident wave, the wave wakes generated by the Pelamis will be perpendicular to the capture wave length (parallel to the Pelamis). The power table presented in Fig. 3 was released by the developer, indicating a maximum wave height of 10 m as the cut-out parameter [62]. However, depending on the conditions of each location and the design parameters of the WEC, it is possible to adjust the cut-out variables for both wave height and period. In the Gulf of Mexico, waves higher than 8 m are only experienced under storm and hurricane conditions, when the WEC will be cut-out from operation [23].

The Vestas V90 3 MW OWTs have been commercially used for more than ten years, and have been installed on different offshore areas with excellent results. It is one of the most widely used OWTs in the world, and its power curve has been provided by the manufacturer as shown in Fig. 4. Air density was considered as a constant at 1.225 kg/m^3. In the area of study including the Caribbean, air density variability was reported as 6% [64]. The Vestas V90 3 MW has a hub height of 80 m, rotor diameter of 90 m, cut-in wind speed of 4 m/s, rated wind speed of 16 m/s, cut-out wind speed of 25 m/s, and restart (cut-back-in) wind speed of 20 m/s. It is also possible to modify existing OWTs by changing their current foundation systems to floating system to be used in different offshore areas [65]. Manufacturers such as Vestas and Siemens [66] are installing its current OWT models on floating foundations [67].

The algorithm was designed with a plug in approach that can easily include or replace the selected devices with other WEC or OWT models in future applications. The proposed wave wake preprocessing method is able to calculate the wakes of those WEC and OWT considering their individual physical characteristics. The power output of each device will be calculated using their individual power tables, and to be seamless integrated into the entire optimization algorithm without major modifications. Likewise, meteorological conditions of diverse geographical locations can be added to the algorithm to perform proper assessment for each specific location. As OWTs grow larger to harvest more energy, occupied areas will be increased so that safety distances between equipment can be assessed and optimized with the new occupied areas.

2.4. Wave wake preprocessing method

One of the major contributions of this research is the introduction of

Tp (s)	3	4	5	6	7	8	9	10	11	12	13	14	15	16	17	18	20
Hs (m)	Hs: wave height (meter) Tp: wave peak period (second)																
0.125	0	0	0	0	0	0	0	0	0	0	0	0	0	0	0	0	0
0.5	0	0	0	0	0	0	0	0	0	0	0	0	0	0	0	0	0
1	0	0	11	27	50	62	64	57	49	41	34	28	23	0	0	0	0
1.5	0	0	26	62	112	141	143	129	110	91	76	63	52	43	36	30	23
2	0	0	66	109	199	219	225	205	195	162	135	112	93	77	64	54	41
2.5	0	7	93	171	279	342	351	320	274	230	210	174	145	120	100	84	65
3	0	91	180	246	402	424	417	369	343	331	275	229	208	173	144	120	93
3.5	0	86	211	326	484	577	568	502	421	394	330	312	260	216	196	164	140
4	105	216	326	394	632	616	583	585	494	454	374	361	339	283	236	197	153
4.5	94	233	371	467	735	744	738	634	626	520	473	390	382	319	299	250	208
5	259	364	469	539	750	750	750	750	644	641	531	482	399	394	330	308	274
5.5	428	497	566	612	750	750	750	750	750	635	642	532	482	400	399	341	322
6	597	630	663	684	750	750	750	750	750	750	616	633	525	476	396	386	329
6.5	750	750	750	750	750	750	750	750	750	750	723	592	617	513	458	430	384
7	750	750	750	750	750	750	750	750	750	750	750	692	566	560	500	474	425
7.5	750	750	750	750	750	750	750	750	750	750	750	748	610	607	542	518	467
8	750	750	750	750	750	750	750	750	750	750	750	750	630	653	584	562	509
8.5	750	750	750	750	750	750	750	750	750	750	750	750	650	699	626	606	551
9	750	750	750	750	750	750	750	750	750	750	750	750	670	746	668	650	592
9.5	750	750	750	750	750	750	750	750	750	750	750	750	691	750	710	694	662
10	750	750	750	750	750	750	750	750	750	750	750	750	711	750	750	738	734

Fig. 3. Power table of Pelamis P2 750 kW [62].

Wind Speed [m/s]	Air Density [kg/m^3]											
	0.97	1	1.03	1.06	1.09	1.12	1.15	1.18	1.21	1.225	1.24	1.27
0	0	0	0	0	0	0	0	0	0	0	0	0
4	53	56	59	61	64	67	70	72	75	77	78	81
5	142	148	153	159	165	170	176	181	187	190	193	198
6	271	281	290	300	310	319	329	339	348	353	358	368
7	451	466	482	497	512	528	543	558	574	581	589	604
8	691	714	737	760	783	806	829	852	875	886	898	921
9	995	1028	1061	1093	1126	1159	1191	1224	1257	1273	1289	1322
10	1341	1385	1428	1471	1515	1558	1602	1645	1688	1710	1732	1775
11	1686	1740	1794	1849	1903	1956	2010	2064	2118	2145	2172	2226
12	2010	2074	2137	2201	2265	2329	2392	2454	2514	2544	2573	2628
13	2310	2382	2455	2525	2593	2658	2717	2771	2817	2837	2856	2889
14	2588	2662	2730	2790	2841	2883	2915	2940	2958	2965	2971	2981
15	2815	2868	2909	2939	2960	2975	2984	2990	2994	2995	2996	2998
16	2943	2965	2979	2988	2993	2996	2998	2999	2999	3000	3000	3000
17	2988	2994	2997	2998	2999	3000	3000	3000	3000	3000	3000	3000
18	2998	2999	3000	3000	3000	3000	3000	3000	3000	3000	3000	3000
19	3000	3000	3000	3000	3000	3000	3000	3000	3000	3000	3000	3000
20	3000	3000	3000	3000	3000	3000	3000	3000	3000	3000	3000	3000
21	3000	3000	3000	3000	3000	3000	3000	3000	3000	3000	3000	3000
22	3000	3000	3000	3000	3000	3000	3000	3000	3000	3000	3000	3000
23	3000	3000	3000	3000	3000	3000	3000	3000	3000	3000	3000	3000
24	3000	3000	3000	3000	3000	3000	3000	3000	3000	3000	3000	3000
25	3000	3000	3000	3000	3000	3000	3000	3000	3000	3000	3000	3000

Fig. 4. Power table of Vestas V90 3 MW [68].

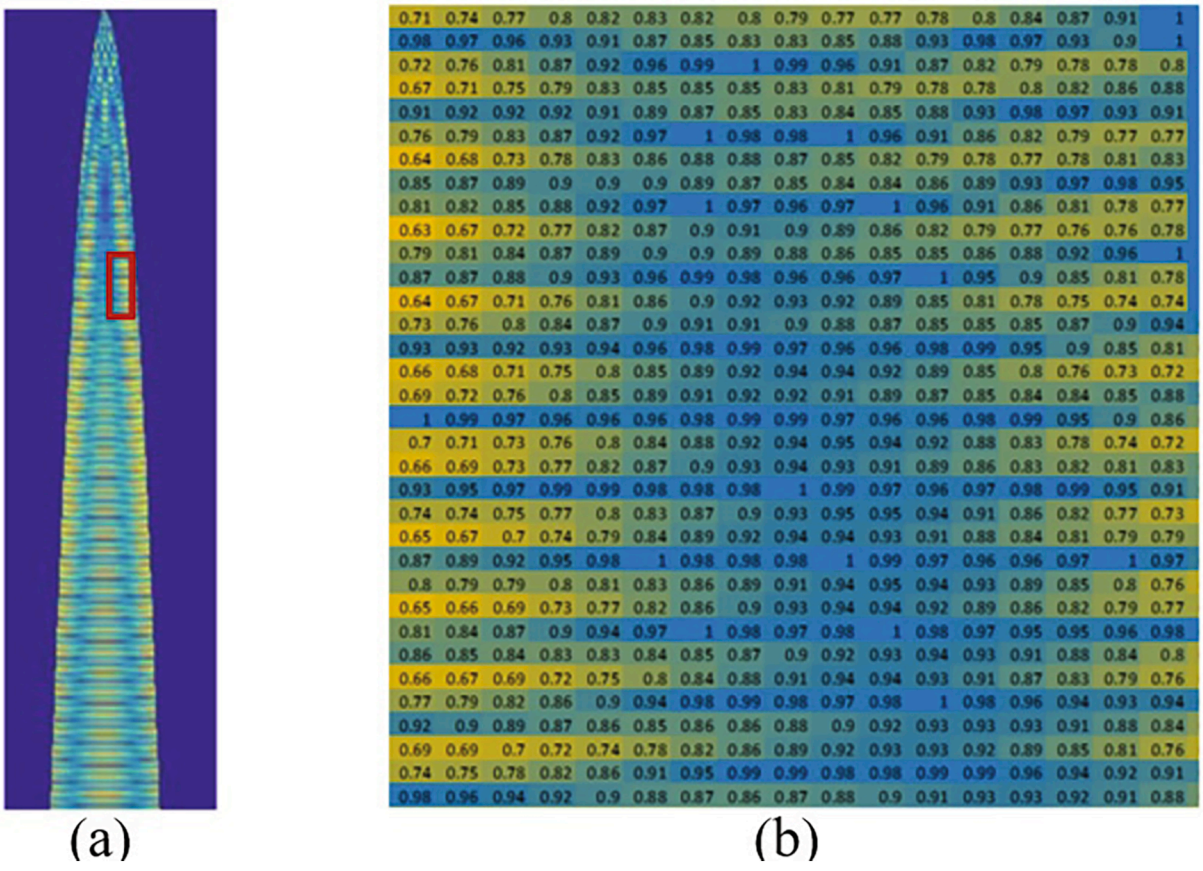

Fig. 5. Graphical representation of grid calculations with (a) extended wake image (b) zoomed in image showing K_d values for each grid location.

preprocessing of the wave wakes to be used a posteriori by different recursive optimization methods. In this paper, genetic algorithm was selected as a demonstration to show the integration of the proposed wave wake preprocessing method and one of the recursive optimization algorithms. Since most recursive optimization algorithms used for layout optimization purpose have similar designs when using a posteriori [69], other common used recursive optimization algorithms, such as particle swarm optimization and ant colony optimization, will be able to use the preprocessed wave wakes. As previously described in Section 2.1, the preprocessing method calculates the wave wake considering the length of the obstacle. The Pelamis WECs were approximated as a series of heaving buoys when considering its capture width. For the OWTs, the diameter of jacket offshore foundation was considered as the length of the obstacle. Sequential bins of diverse wave meteorological conditions were evaluated to calculate K_d, as indicated in Section 2.1, in a grid with a resolution of one meter by one meter. An example of graphical representation of these grid calculations are shown in Fig. 5.

Results from these analysis were stored in computer files with the HDF5 format to be retrieved on the execution of the recursive layout optimization algorithm. Considering the wave directions of the location, the stored grid with K_d values was adjusted for the correct angle applying rotation of matrices in as indicated by Eq. (24) [70]

$$\begin{bmatrix} \cos\theta & -\sin\theta \\ \sin\theta & \cos\theta \end{bmatrix} \begin{bmatrix} x \\ y \end{bmatrix} = \begin{bmatrix} x' \\ y' \end{bmatrix} \tag{24}$$

Where (x,y) are the coordinates on the original preprocessed stored grid, and (x', y') the new position of the rotated K_d value, according to the meteorological wave direction. An overall flowchart of the proposed wave wake preprocessing method is presented in Fig. 6. The locations of each device under each iteration of the recursive algorithm is matched with the prepossessed wave wake stored grid, in the form of HDF5 matrices, which has been rotated in accordance with the wave direction, as required. When the wave wakes overlap with each other, equations listed in Section 2.1 were used to calculate combined wave wakes, which was conducted as part of recursive optimization processes instead of preprocessing. When using new energy devices with different physical characteristics or wave conditions change due to the location change, a new grid of K_d values should be calculated in the preprocessing before conducting the recursive optimization, which makes the proposed concept easy to be adopted by other optimization algorithms.

2.5. Layout optimization method

The layout optimization method selected for this study is the Genetic algorithm (GA). It was implemented in conjunction with novel preprocessing for wave wakes to optimize the layout of a hybrid energy farm. In this approach, the WECs are evaluated as major energy devices while the OWTs are assessed as secondary energy devices. It is relevant to reiterate that preprocessing of wave wakes may be applied to other wave layout optimization algorithms, not just GA. The objective function of the proposed GA based layout optimization method is to maximizing the total power output of the entire energy farm while keeping majority of energy devices as WECs. Both wind wake caused by OWT blades and wave wakes caused by WECs and OWTs' foundations were considered when calculating the power output. Historical meteorological data between 1979 and 2015 from NOAA WaveWatch III system was used while safety distance constraints were also considered during the optimization process.

To ensure the majority of energy devices in the hybrid energy farm as WECs, the modified GA was able to handle two different sets of initial individuals through the optimization process. As indicated in Fig. 7, two sets of random individuals representing layouts with WECs only (set A) and OWTs only (set B) were initiated. Within each set, the individuals were numbered from 1 to A (or 1 to B for OWTs only), and the individuals from both sets with same numbering were combined to create layouts with both WECs and OWTs. Safety distances and restricted area rules, which were discussed in detail later, were applied to the combined layouts to eliminate energy devices that did not meet either of the rules. The modified combined layouts were then separated into two sets of individuals again, one with remaining WECs only and the other one with remaining OWTs only. The power output (fitness function) of each separated layout was calculated, and the two sets of individuals went through selection, crossover and mutation processes. New random individuals were re-inserted into each set to keep same number of individuals for each generation. If the predefined maximum generation was reached, the optimal layout would be extracted from the results. Otherwise, the optimization process was repeated until reaching the maximum generation. The K_d values generated by different types of obstacle(s) (WEC only, OWT only, WEC with WEC, WEC with OWT, and OWT with OWT) at all possible locations under possible wave conditions were calculated first in preprecessing stage and stored in a separate database, which was uploaded to the computer memory for its application on calculating the power output of WECs. The application of the preprocessed K_d values allowed to compute the wave height available for each WEC.

A 4,000 m by 4,000 m area was chosen as available area for the hybrid energy farm. The area was divided into 6,400 cells with 50 m by 50 m size. The center of each cell was considered as one possible location to put an energy device, so there were 6,400 possible locations where a WEC or an OWT might be installed. Each individual in the GA, represented a possible layout, was a chromosome with length of 6400 ones and/or zeros, where one indicated a device installed while zero indicated no device installed on the specific cell. Each generation was composed of two sets of 600 individuals (A = B = 600). The power output (fitness function) of each modified layout was calculated applying the corresponding power table of selected energy device and historical meteorological data to the modified layout. The individuals in each set were ranked in descending order based on total energy output for selection process. The capacity factor (CF) of each device in a layout was also calculated to be used as evaluation and comparison criteria beside total power output. In this study, the following GA parameters were used: selection rate = 0.9, crossover rate = 1.0, mutation rate = 0.01, number of individuals in each generation = 600, and maximum generations = 500.

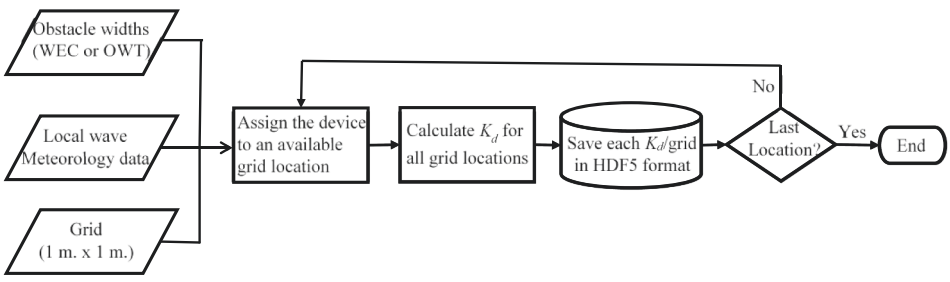

Fig. 6. Overall flowchart of the proposed wave wake preprocessing method.

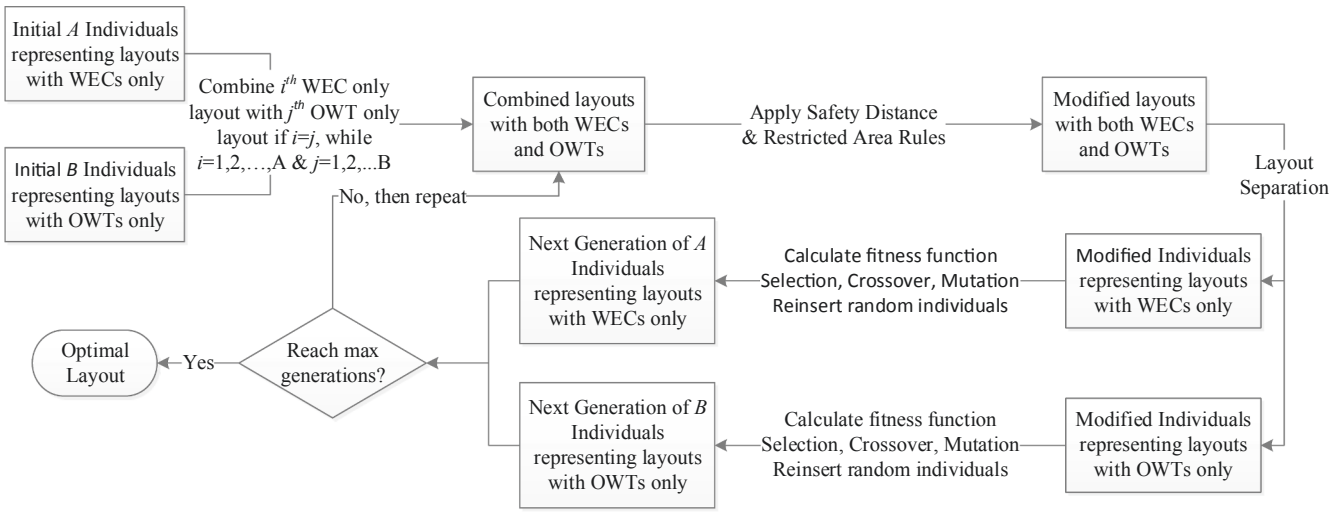

Fig. 7. Flowchart of the new GA based layout optimization method.

2.5.1. Different approaches for applying safety distance rule

The minimum distances between the devices must be no less than the safety distance of the device in a feasible layout of any energy farm. Before calculating the power output of any layout, each combined layout (with both WECs and OWTs) was modified by removing any devices in the layout that violated the safety distance rule. The Pelamis P2 750 kW WEC could rotate 360° with respect to its anchor and adjust itself to be parallel to the direction of incident waves. Adding the slack of the anchor cables for the WEC, the safety distance of a Pelamis P2 750 kW WEC was assumed as 600 m considering the length of the WEC (180 m), clearance and slack on the cable. This safety distance was assumed to ensure low risk and to avoid collisions, considering the mobility that anchor cables generate for the WECs. The safety distance of the OWT was considered as 450 m (five times of its rotor diameter 90 m). The basic idea of applying safety distance rule was to select a device (called anchor device) and remove any other devices within the safety distance range of the selected anchor device. One anchor device was selected each time, and the approach was repeated to select next anchor devices for applying safety distance rule until all remaining devices meet the safety distance rule. There are different approaches to select the anchor devices. Three major approaches were conducted to select anchor devices as described below during pre-testing, and chose the best approach for using in the case studies.

1) Completely random based selection. The first and all other anchor devices were completed randomly selected from the remaining devices (except previous selected anchor devices).
2) Reference point based selection. The anchor device was chosen as the one closest to a reference point among all remaining devices (except previous selected anchor devices). Different methods were tested for choosing reference point:
   a. Changing reference points: The first reference point was chosen as the origin of the layout (left lower corner), and the next reference point was then chosen as last anchor device.
   b. Fixed reference point: The reference point was always chosen as the origin of the layout, while the anchor devices were chosen based on the distances to the origin.
3) Dominating wave or wind direction based selection. The dominating wave or wind direction was identified from historical meteorological data. The first anchor device was chosen as the one that was first impacted by the dominating wave or wind direction. The next anchor devices were chosen as:
   a. The device closest to last anchor device among all remaining devices except previous selected anchor devices, or

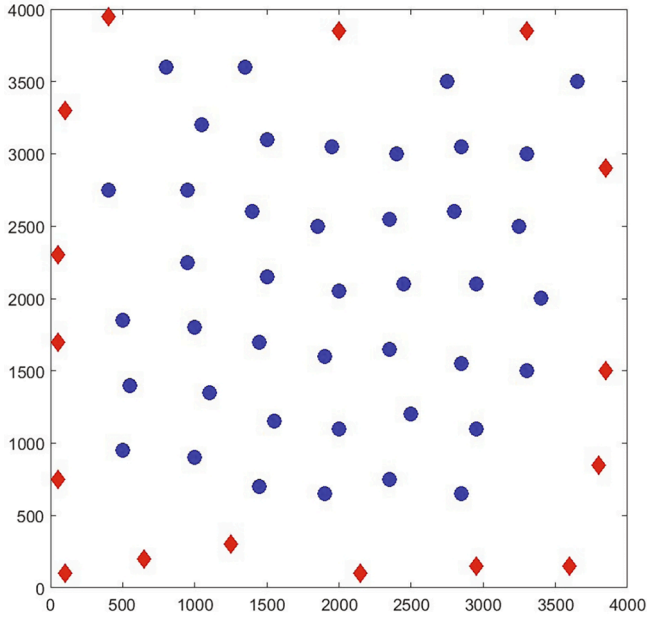

Fig. 8. One of the best layouts generated in pre-test using safety distance rule only, in which blue circles represent OWTs and red diamonds represent WECs.

   b. The device closest to the first anchor device among all remaining devices except previous selected anchor devices.

If there were two options or more for anchor device, the one closest to the origin was chosen as the next anchor device. Based on pre-testing results, which was presented in next section, the approach that used dominating wind direction and closest to the first anchor device as criteria to choose anchor devices had the best performance among all the methods described above. It was then used in the case studies below.

2.5.2. Different approaches for applying restricted area rule

Since OWTs' safety distances are short than those of WECs, it is possible that OWTs may occupy a larger proportion of the given area under the optimized layout, which would not keep WECs as major energy device in the hybrid energy farm. During pre-testing process, it was found out that the layouts with safety distance rule only showed OWTs occupied most of the area while WECs were only placed along the border of the layouts. One of the best layouts with safety distance rule only from

pre-testing is shown in Fig. 8. Since only the safety distance rule was applied in the pre-testing process and OWT's safety distance is 25% less than the WEC's safety distance, the optimization process placed more OWTs closer in the pre-testing process while leaving no enough spaces for WECs. Another possible reason could be that GA intended to select the layouts with more high power output devices while OWTs had higher nameplate capacity than WECs.

In order to balance the number of WECs and OWTs and keep WECs as the major energy devices in the optimized layouts, a restricted area rule was created and added in the optimization process in addition to the safety distance rule. The restricted area rule only allows OWTs to be only placed in a certain area within the entire layout while WECs were allowed to be placed anywhere in the entire layout. The size of restricted area was chosen as one fourth of the total area, which is 2000 m by 2000 m. Five different options of placing the restricted area were tested in the pre-testing including four corners and the center of the layout. The center location was chosen as the restricted area in the case studies based on the pre-testing results. A reference case study without OWT and WEC interaction was not used to evaluate this optimization method, since the layouts of hybrid energy farm and WEC only energy farm would be different. For a WEC only energy farm, WECs would be organized in rows and columns under a rectangular area, which would make the comparison with the hybrid energy farm unfeasible. Additionally, the WECs do not generate wind wakes to decrease standalone wind power generation, while the main wave wakes would be generated by WECs instead of the foundations of OWTs.

3. Studying area and pre-testing

The Gulf of Mexico (GoM) was selected for the testing of the new wave wake preprocessing method coupled with recursive GA optimization considering that previous studies have indicated that there is a significant wave and wind resources in the area. Meanwhile, the energy devices in most areas of the GoM do not need to suffer extreme energetic oceanic conditions that exist on other locations [23]. These extreme energetic ocean conditions require more expensive WEC designs to withstand those conditions [16], as several WECs have been damaged or destroyed in the past [13]. Furthermore, the GoM has a large electricity consumer base both on the coastal and offshore areas, with one of the largest oil and gas offshore platforms concentrations in the world and several of the largest cities in the US close to its littorals [23]. It should be noted that not every offshore location is suitable for building a wave-wind hybrid energy farm. The potential capacity factor (CF) of each device in the GoM was analyzed to choose potential case study areas and considered it as selection criterion. Since Vestas V90 has a nameplate capacity of 3 MW while Pelamis P2′s nameplate capacity is 750 kW, a combination of four Pelamis P2 with one Vestas V90 (total 6 MW) was considered to be placed in each grid (one sixth longitude by one sixth latitude) for evaluating the capacity factor. The wake effects from wave and wind were not considered during the location selection process.

Historical meteorological data from the WaveWatch III system provided by NOAA was used. The data included wind speed (at 10 m. height in u and v vector format), significant wave height (Hs), dominant wave period (Tp) and wave direction given on nautical notation, where zero indicates waves propagating from the North [71]. The data is from 1979 to 2015 with temporal resolution of 3 h and the spatial resolution of one sixth of a degree. The best locations in terms of capacity factor were evaluated as shown in Fig. 9. Capacity factor was computed as the average power output of the combination of devices divided by its combined nameplate capacity (6 MW). Fig. 9 shows that the best areas in terms of CF value to develop a wave-wind hybrid energy farm are on (1) the northwest section of the GoM (Coastal Bend of Texas) with CF up to 31% and (2) the Strait of Yucatan with some locations close to the coast up to 31% CF. The yearly average power output of the combination of devices were shown in Fig. 10, which shows the two sections with highest CF values identified in Fig. 9 also have highest yearly average power output.

One of the main challenges of wave energy is its significant variability [22]. Studies have indicated that combining wave energy with wind generates many synergetic benefits [23]. One of those benefits is reducing wave energy variability [27] and therefore improving its harvesting logistic and integration to the grid [26]. Therefore, an

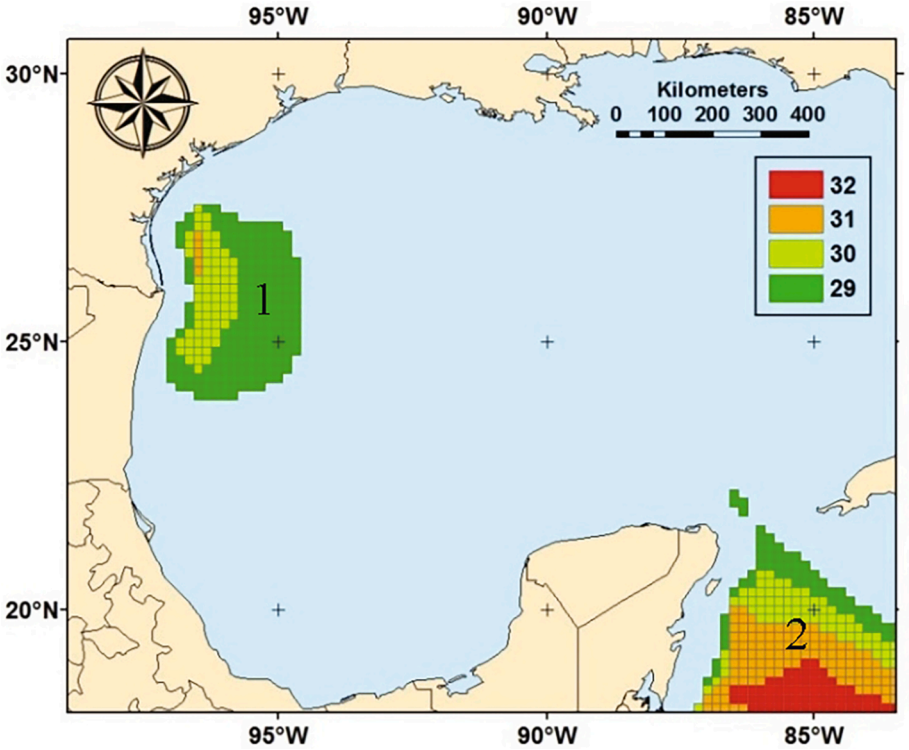

Fig. 9. Locations in the GoM with capacity factor higher than 29% for the combination of four Pelamis P2 and one Vestas V90.

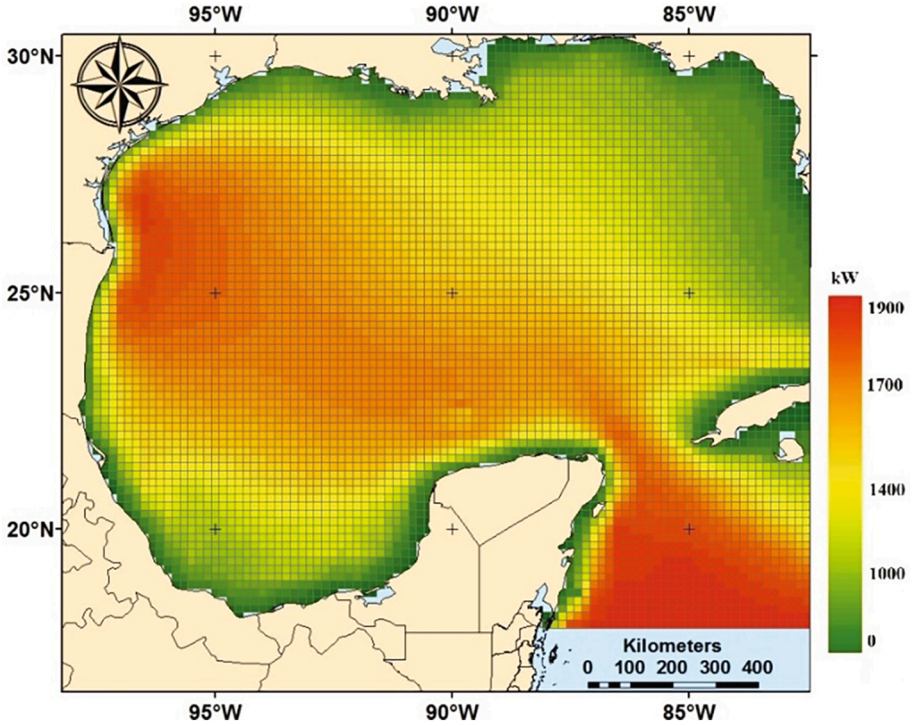

Fig. 10. Yearly average power output of the combination of four Pelamis P2 and one Vestas V90 in the GoM.

Table 1
Wind and Wave Energy Generators Combinations with 12 MW rated power output 12 MW according to equipment Nameplate Capacity.

	100% wave	75% wave – 25% wind	50% wave – 50% wind	25% wave – 75% wind
# of Vestas	0	1	2	3
# of Pelamis	16	12	8	4

additional criterion applied to evaluate the optimal placement for the proposed layouts is identifying the locations where the combination of wave and wind maximizes variability reduction in the GoM. The GoM has been previously studied to evaluate the advantages of combination of wave and wind wave resources and results have indicated that a significant variability reduction is obtained [23], coupled with the maximization of the assigned areas and the installation, operation and maintenance cost reduction for the combined installation [25].

Four diverse combination arrays were evaluated to assess wave resource variability reduction from collocation of WECs and wind turbines as indicated in Table 1 with a total power output of 12 MW. Different numbers of WECs and OWTs were considered for each option to account for the diverse nameplate capacity (NPC) of the devices involved. No wake losses are considered for this particular array.

Wave and wind power outputs were calculated for each location and time period from the Wave Watch III system meteorological data provided by NOAA. Standard deviation and Coefficient of Variation (Cv) were calculated for each location data point, considering the complete time interval. Results were exported to GIS to perform geospatial analysis for the variability data as shown in Fig. 11. Results indicate that wind energy reduces variability for wave energy in the GoM. The introduction of 25% wind energy in the layout (Fig. 11b) reduces variability for two locations: (1) the Northwest section of the GoM and (2) the Strait of Yucatan. The variability reduction reported for the Coastal Bend area of Texas is relevant considering that this area also has high CF as reported in Fig. 11. The second location on the Strait of Yucatan is also important considering that indicates both high CF and high variability reduction. Furthermore, as observed on Fig. 11c and d, as the wind resource increases in the mix the reduction of the Cv increases on extended locations of the Texas coast and the Yucatan Peninsula. These analyses validate both locations as providing the highest wave energy variability reduction in the GoM when wind energy is introduced in the layout.

Based on the results shown in Figs. 9, 10 and 11, two specific locations were selected as case study areas as indicated in Fig. 12. The first location was identified as the Coastal Bend Texas location at Latitude 27 and Longitude −96.5, with water depth of 200 m. The second location was identified as Yucatan Strait location at Latitude 20 and Longitude −86.5, with water depth of 500 m. The Coastal Bend Texas location was initially considered to evaluate the performance of the proposed GA method including pre-testing stage, while the Yucatan Strait location was used to validate the GA method.

3.1. Pre-test results

Pre-test was conducted to compare different approaches related to apply safety distance rule and restricted area rule as described in Sections 2.5.1 and 2.5.2. The Coastal Bend Texas location and its corresponding meteorological data were used in the pre-test stage. In the pre-test stage, December and July were chosen as the selected months representing high potential winter months and low potential summer months. The rest GA parameters were same as described in Section 2.5.

The study first tested different approaches for applying safety distance rule. It should be noted that the restricted area rule was not applied yet when testing these safety distance rule approaches. The first approach was completely random based selection. The convergence curves of fitness function of the GA based method are shown in Fig. 13, where green line indicates maximum power output and blue line indicates average power output of all layouts in that generation. The results indicate that the completely random based selection approach did not show any convergence or improvement over 500 generations.

The second and third approaches tested were reference point based selection including changing reference points and fixed reference point,

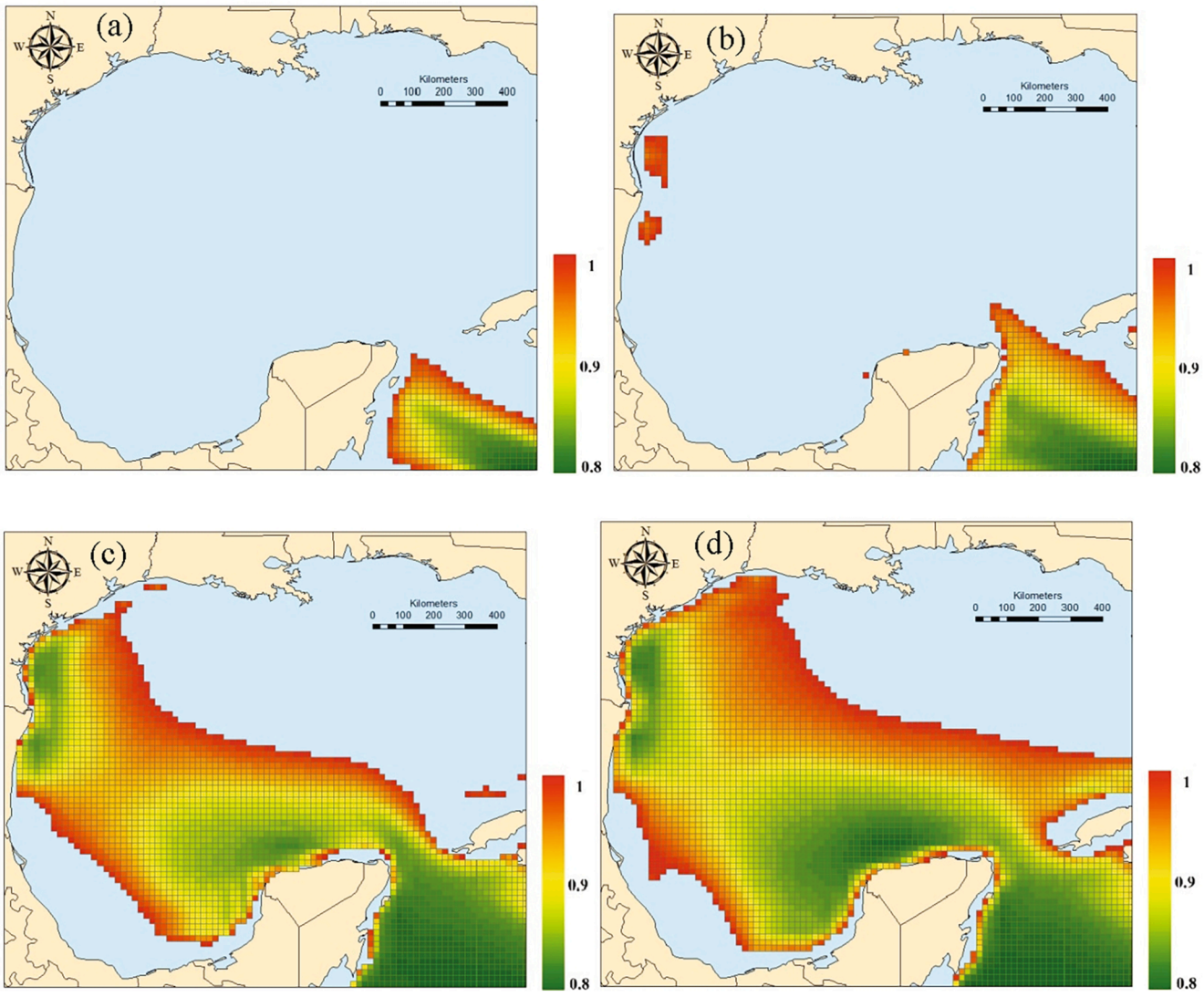

Fig. 11. Coefficient of Variation less or equal than one on combinations of wave and wind energy generated by Pelamis WEC and Vestas V90 3 MW in combinations of (a) Wave 100% Wind 0% (b) Wave 75% Wind % 25% (c) Wave 50% Wind 50% (d) Wave 25% Wind 75%.

and their results are shown in Figs. 14 and 15. The results show some level of convergence for the average power output in both figures. However, the maximum power output curve of changing reference points approach (green lines in Fig. 14) do not show any obvious convergence, while the fixed reference point approach shows better results in both convergence and power output values. So there are improvements on both maximum power output and average power output results of fixed reference point bases selection approach compared to the changing reference points approach.

The last two approaches tested are dominating wind direction based selection including changing reference points and fixed reference point. The results are shown in Figs. 16 and 17. Compared to previous approaches, the last two approaches show much better results in term of convergence. The last two approaches considered the variability on the wind direction, and the anchor device would have the least impact from the wakes, which means the potential best performing devices may be kept during the elimination process. Meanwhile, the dominating wind direction and fixed reference point based approach (Fig. 17) also show highest power output values in both maximum and average power output among all the tested approaches. It was decided to choose the dominating wind direction and fixed reference point based selection as the final approach to apply safety distance rule in the case studies.

After choosing the final approach for applying safety distance rule in the GA based optimization method, different restricted area locations as discussed in Section 2.5.2 were also tested in the pre-test stage. Since the restricted area rule was mainly to keep WECs as major energy devices, the CF values of WECs in the optimized layout for each possible restricted area location are shown in Fig. 18 and compared to choose the final location for placing the restricted area. The center location is the best location with almost 50% of WECs having CF 18% or higher while the other options generated layouts with most WECs having lower CF. If the restricted area was placed on any of the borders of the layout, the WECs on the interior had a significantly lower power generation since the OWTs on the edges blocked WECs that otherwise could produce higher CF. Therefore, the center of the layout (4,000 m by 4,000 m) was chosen as the location to place the restricted area (2,000 m by 2,000 m) in the case studies. So the OWTs would be only placed within the restricted area after applying the restricted area rule leaving a margin area on the perimeter of the layout where OWTs were not considered for placement. Meanwhile, the WECs could be placed anywhere in the entire layout to increase the possibility of receiving more energy on possible locations. However, for a given area that has wave from a predominant direction, other options to place the restricted area may generate better results.

Once the approaches for applying safety distance rule and restricted area rule were decided, the GA based optimization method would work

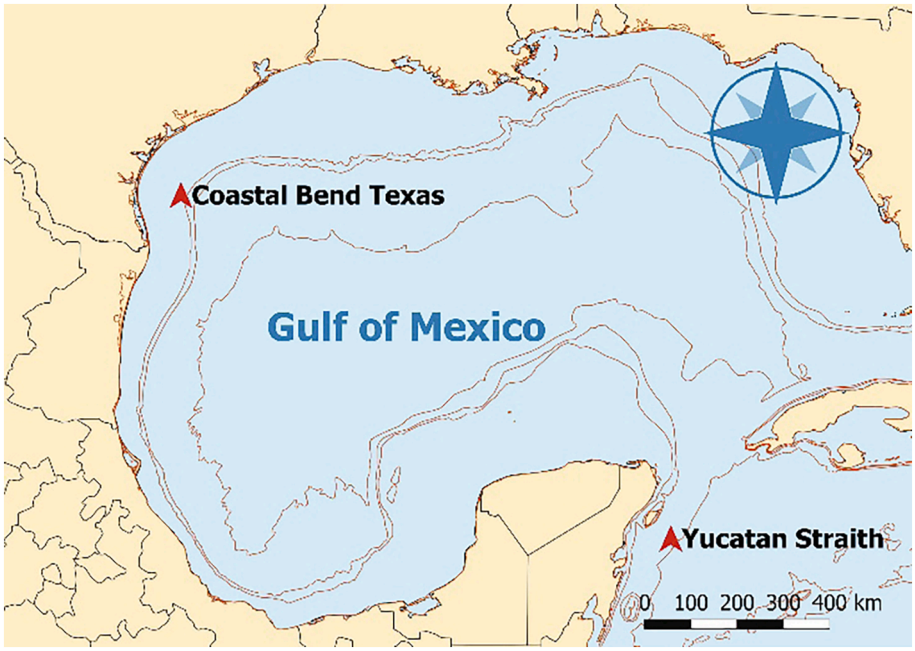

Fig. 12. Map of two specific case study locations.

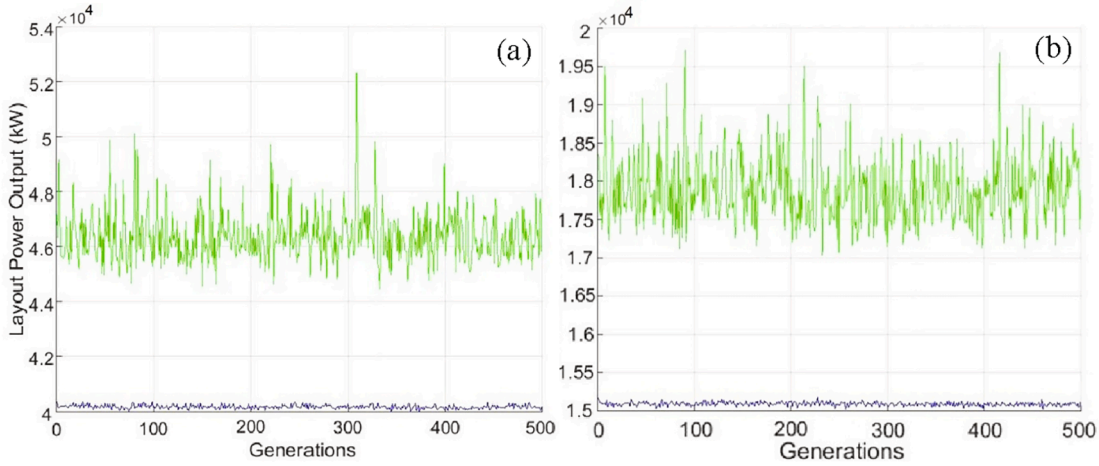

Fig. 13. Fitness function curves of pre-test using completely random based selection approach for applying safety distance rule, where green line indicating maximum power output and blue line indicating average power output of all layouts in that generation: (a) December and (b) July.

as indicated in Fig. 7. For calculating OWT's power output, the possible wind speeds were divided into 1 m/s bins from 0 to 25 m/s while the possible wind directions were segmented into bins of 10° size from 0° to 360°. A two dimensional matrix with 925 elements was created, in which each element represented a possible combination of wind speed and wind direction. For the WEC, three factors will influence its power output, including significant wave height (*Hs*), dominant wave period (*Tp*) and wave direction. A 3D matrix was created, considering *Hs* with the range from 0 m to 8.5 m in 0.5 m increments, *Tp* with the range from 0 s to 17 s in 1 s increments, and wave direction with the range from 0° to 360° in 10° increments. The 3D matrix had 11,988 elements to represent the possible combinations of all meteorological factors for wave power calculation. Using the matrices, it was possible to significantly reduce computational expenditure when calculating the power outputs and wakes. The GA based optimization method used about 270 s to execute each generation, in which 150 s were devoted to the evaluation of the wave wakes from both wind turbine foundations and WECs. Nevertheless, it's important to consider that significant reductions in computational expenditure were obtained applying preprocessing of wave wakes and use of the K_d databases since it took about 78 min to calculate all possible K_d values under one wave condition.

4. Case studies and results

The new wave wake preprocessing concept, coupled with GA based layout optimization approach, was tested in two case studies to validate the proposed concept. Safety distance and restricted area rules were applied for layouts with total area of 4,000 m by 4,000 m considering 36 years (1979–2015) of historical meteorological data from WaveWatch III.

4.1. Case study 1: Coastal Bend Texas location

The optimal layout for a wave-wind hybrid energy farm in Coastal Bend Texas location (Fig. 12) is shown in Fig. 19. This layout indicates a number of WECs with yearly average CF above 20% and more than 75%

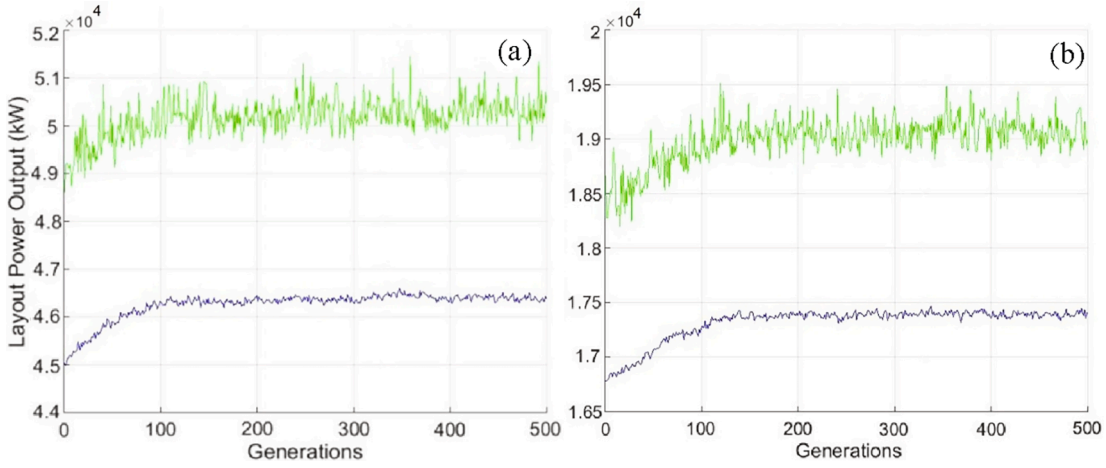

Fig. 14. Fitness function curves of pre-test using changing reference points based selection approach for applying safety distance rule, where green line indicating maximum power output and blue line indicating average power output of all layouts in that generation: (a) December and (b) July.

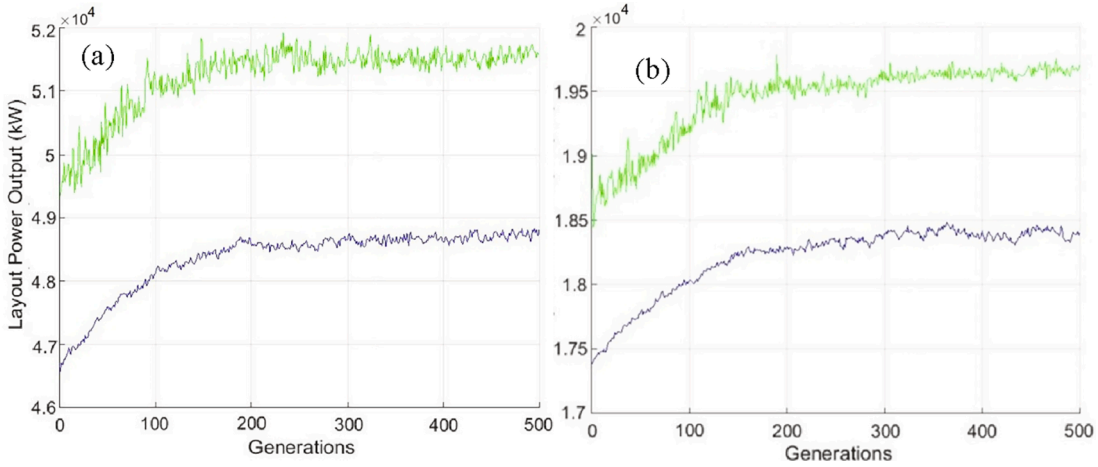

Fig. 15. Fitness function curves of pre-test using fixed reference point based selection approach for applying safety distance rule, where green line indicating maximum power output and blue line indicating average power output of all layouts in that generation: (a) December and (b) July.

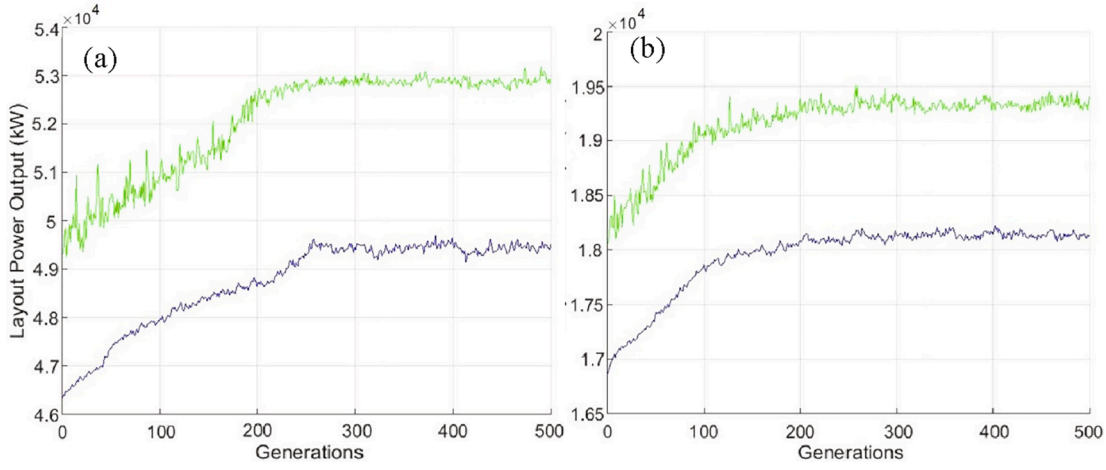

Fig. 16. Fitness function curves of pre-test using dominating wind direction and changing reference points based selection approach for applying safety distance rule, where green line indicating maximum power output and blue line indicating average power output of all layouts in that generation: (a) December and (b) July.

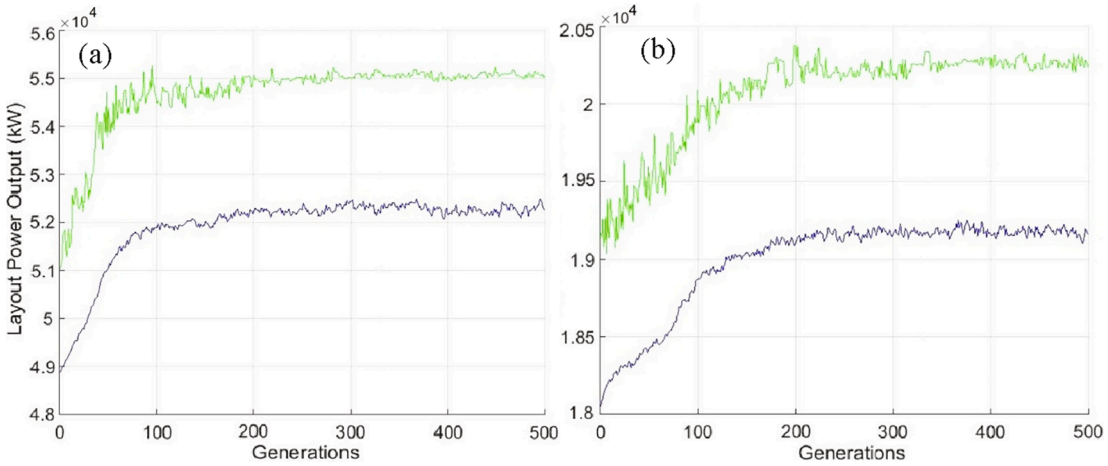

Fig. 17. Fitness function curves of pre-test using dominating wind direction and fixed reference points based selection approach for applying safety distance rule, where green line indicating maximum power output and blue line indicating average power output of all layouts in that generation: (a) December and (b) July.

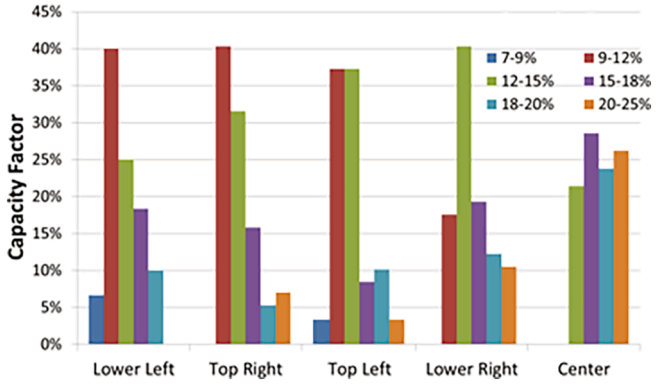

Fig. 18. Capacity factor values of all WECs in the optimized layouts based on different the restricted area locations in the GA based optimization method in pre-test stage.

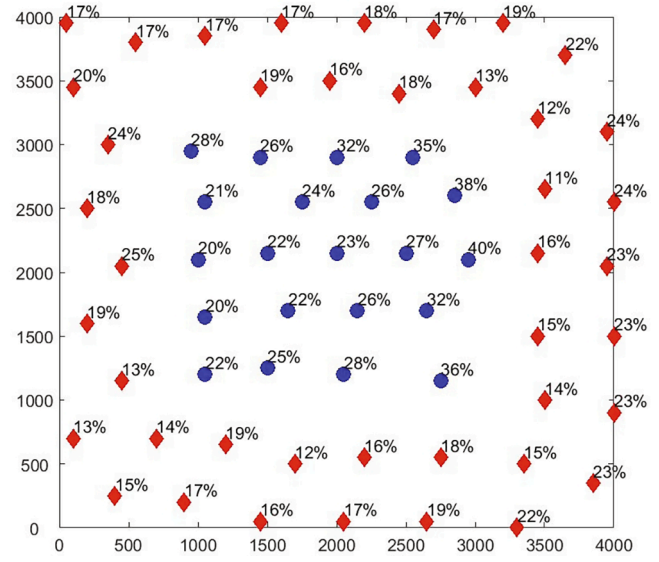

Fig. 19. Optimal layout for a wave-wind hybrid energy farm in Coastal Bend Texas location identified by the GA based layout optimization method, where red diamonds represent WECs and blue circles represent OWTs.

of WECs have yearly average CF higher than 15%. On the other hand, all of the OWTs have yearly average CF higher than 20% while more than 20% OWTs have yearly average CF above 30%. These results are very promising since the commercial threshold for OWT's CF has been considered as 30% [72] with fluctuation from 20% to 30% due to inter year variability [73], while a 20% CF was considered adequate for the Pelamis 750 kW by previous research [22] .

The yearly average CF value distribution among the devices is shown in Fig. 20. It indicates that more than 50% of WECs have at least 20% yearly average CF while less than 10% of WECs have a yearly average CF lower than 14%. Considering that these CF values are yearly averages and the seasonal variation of wave energy in the GoM, it indicates that the WECs have very good monthly average CF in a number of months to get the 20% yearly average CF. On the other hand, results for the wind turbines yearly average CF indicate that almost 30% of the OWTs have yearly average CF values on the ranges of 30–40%, which exceeds the upper limit of the commercial thresholds. Meanwhile, the rest of OWTs operate above 20% yearly average CF, which are acceptable values considering the inter year variation of the wind resources.

The fitness function curves are shown in Fig. 21, where green line represents the maximum power output and blue line represents average power output in that generation. The power output of the WECs becomes stable after around 300 generations, while the power output of the OWTs becomes stable after around 150 generations.

4.2. Case study 2: Yucatan Strait location

To further validate the effectiveness of the new preprocessing wave wake method, coupled with GA based optimization approach, the second location, Yucatan Strait location (Fig. 12), was chosen as case study to test the method. The Yucatan Strait location has different meteorological conditions compared to the Coastal Bend Texas location according to previous literature [23]. Therefore, it would be important to evaluate if the GA based optimization method performs adequately on the second location. After 500 generations, the optimal layout (Fig. 22) was identified for a given area of 4,000 m by 4,000 m in the Yucatan Strait location. It shows similar performance as the previous case study layout (Fig. 19), but it has slightly more devices with three more OWTs and one more WEC installed on the layout. The different arrangement of the devices indicate the influence of the diverse weather patterns (wave and wind) on the power output and therefore on the layout distribution. Almost 42% of WECs generate yearly average CF higher than 20% while more than 90% of WECs generate yearly average CF of 13% or higher. Considering the inter year variation and the seasonal behavior of the GoM area, these CF values are encouraging for development of wave energy harvesting.

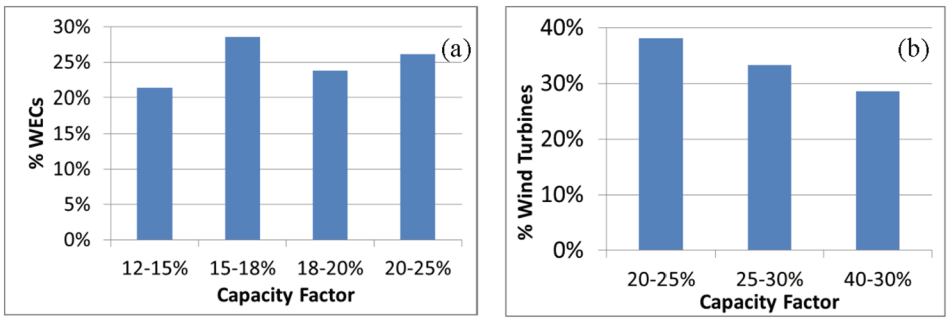

Fig. 20. Histogram of yearly average CF of (a) WECs and (b) OWTs in the optimal layout of Coastal Bend Texas location.

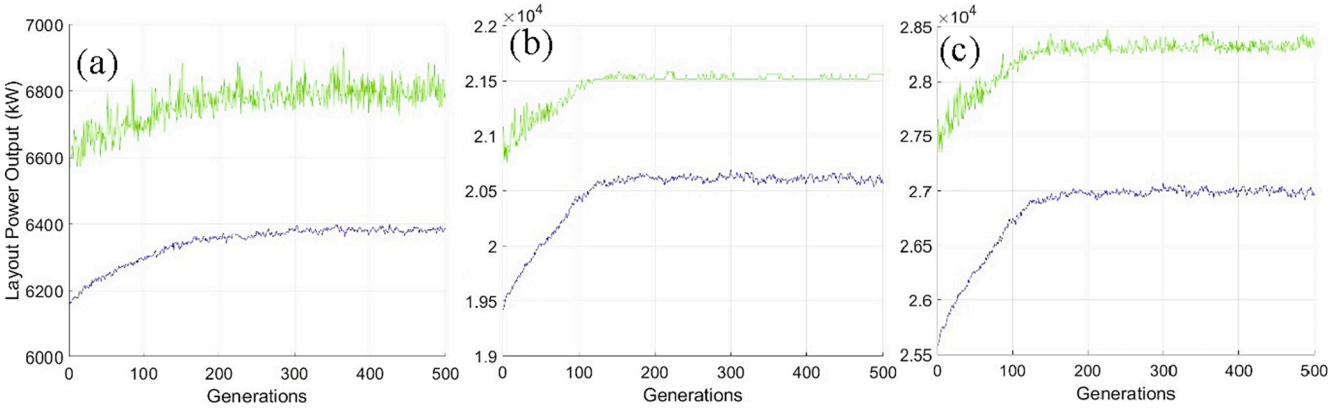

Fig. 21. Fitness function (power output) curves of the Coastal Bend Texas location: (a) WECs, (b) OWTs, and (c) Total.

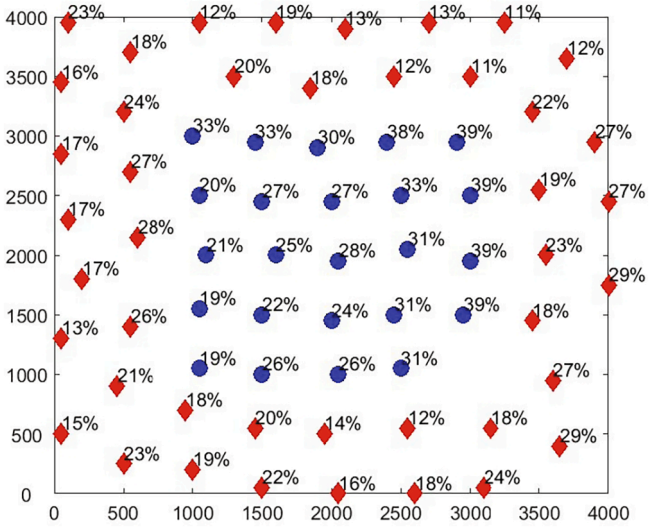

Fig. 22. Optimal layout for a wave-wind hybrid energy farm in Yucatan Strait location identified by the GA based layout optimization method, where red diamonds represent WECs and blue circles represent OWTs.

The yearly average CF values of the WECs and OWTs on optimal layout (Fig. 22) are shown in Fig. 23. Almost 20% of the WECs have higher than 25% CF values, and less than 10% WECs generate less than 13% CF, which indicates a good performance for the optimal layout. On the other hand, the number of wind turbines installed increased by three when compared with previous case study. Almost 50% OWTs have 30% or higher CF values. The results further validate the effectiveness of the GA based optimization method.

To further validate the performance of the wave wake preprocessing method, coupled with GA based optimization, the fitness function curves are presented in Fig. 24. The average power output of WECs (blue line on Fig. 24a) shows more than 250 kW improvement after optimization process, while the maximum power output of WECs (green line on Fig. 24a) shows almost 300 kW improvement after optimization. On the other hand, both the average and maximum power outputs of OWTs show more than 1 MW improvement after optimization process (Fig. 24b). The second case study with different location and meteorological conditions offers further validation on the effectiveness of the GA based layout optimization method for a combined wave and wind energy farm.

These case studies indicated that the proposed approach applying the new wave wake preprocessing method is capable of practical application on the development of hybrid wave-wind energy farms. Furthermore, considering that a plug-in approach was applied in this research, the optimization algorithm is able to consider other WECs and OWTs models without major changes in the methods. Considering that the Pelamis is one of the most studied WECs and a large number of its design data and benchmark results are available [9], their application for this research aided in the development of the optimization algorithm. Nevertheless, other WECs may be incorporated in the future to evaluate similar layout optimization processes. Preprocessing would be carried out for these diverse WECs models to calculate the wave wakes, based on their specific parameters and operational data, incorporating them to the algorithm.

5. Conclusion

Wave energy is still in research and development stage, with no large commercial application, after more of 40 years of investment. This is concerning considering that previous studies have indicated that wave energy could supply a considerable portion of the world's electricity demand. To incentivize the development of this valuable renewable

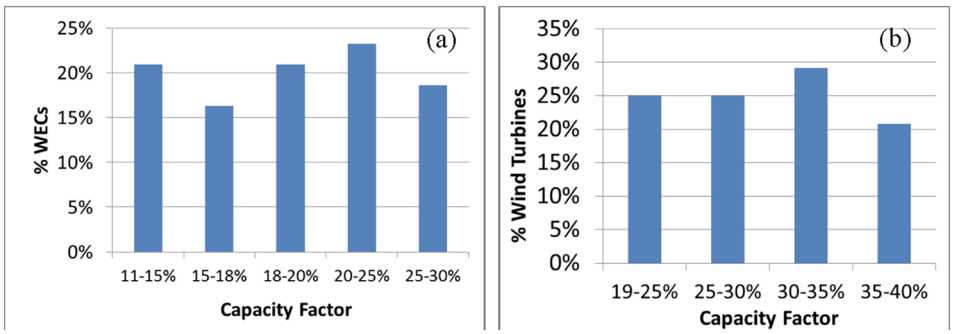

Fig. 23. Histogram of yearly average CF of (a) WECs and (b) OWTs in the optimal layout of Yucatan Strait location.

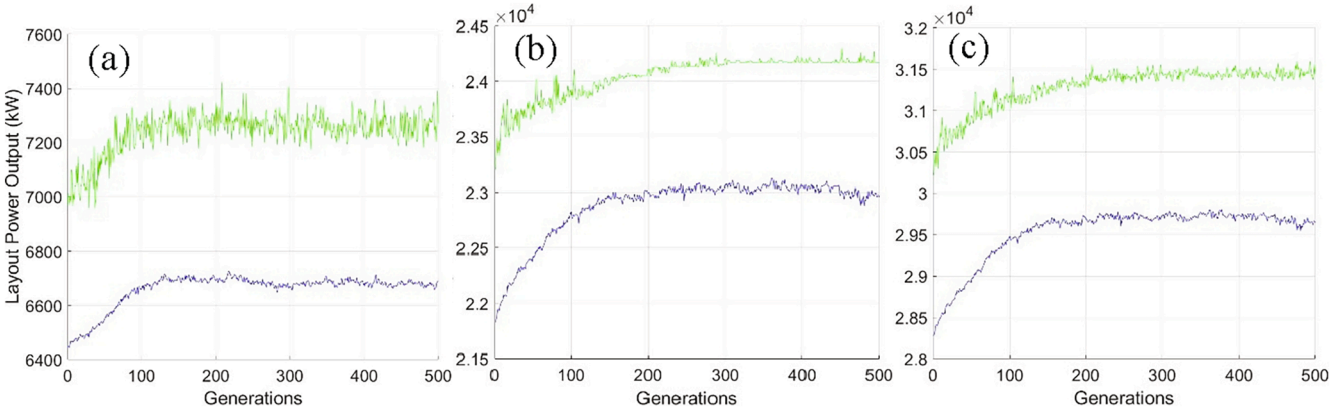

Fig. 24. Fitness function (power output) curves of the Yucatan Strait location: (a) WECs, (b) OWTs, and (c) Total.

energy resource, previous research has pointed to the development of hybrid wave-wind farms. These installations would generate a large number of synergetic benefits, including variability reduction, decreasing installation and operational cost, better utilization of marine areas and overall increase on energy extraction. However, two main challenges have been identified in the development of hybrid wave-wind farms. The identification of locations possessing adequate wave and wind resources while simultaneously reducing the risk of equipment damage caused by extreme oceanic conditions. The second challenge is the development of layout optimization algorithms capable of handling the complexity of wave wakes caused by the combined equipment, at reasonable processing times. This research introduced a new wave wake preprocessing concept to evaluate wave wakes. The extremely time consuming wave wake calculations are performed in advance of the execution of the recursive layout optimization algorithms, with results saved in physical medium to be accessed in each iteration by the optimization algorithm. The research addressed previously indicated challenges, creating an efficient optimization algorithm based on wave wake preprocessing concept, which was successfully tested in two case studies.

Geospatial analysis was first applied to evaluate diverse locations in the Gulf of Mexico on their fitness for a hybrid wave-wind farm. Maximization of combined power output and minimization of wave-wind power variability were both considered to select the locations for the case studies. The area has been characterized by previous research as possessing adequate wave-wind power while reducing risk of equipment damage due to rough sea conditions. The research introduced a layout optimization algorithm for a wave-wind hybrid farm. To overcome challenges presented by lengthy wave wake calculations, preprocessing was incorporated. The wave wake model was integrated to the optimization process through a preprocessing stage, which contributed to reduce computational time and expenditure. Safety distance and restricted area rules with two sets of populations were developed in the genetic algorithm to identify the optimal layout in which WECs are kept as the major energy devices. Both wind and wave equipment interaction are considered in the optimization algorithm to maximize the power output by reducing the wake interferences. Over 36 years (1979–2015) historical meteorological data in two selected locations were used to validate the new method. The efficient computational approach applied was able to handle all the big data and wake effect calculation with acceptable computational time.

Two locations in the Gulf of Mexico, which have good potential for collocating WECs and OWTs, were chosen as case studies. Although the meteorological conditions in both locations are different, the results in both locations are promising with significant improvements on the power output. In the optimal layouts, a large proportion of the energy devices generated capacity factors values above commercial thresholds. The Coastal Bend location generates CF between 15% – 20% for many of the WECs, while the OWTs have yearly average CF above 20% with more than 20% of the turbines higher than 30%. In the Yucatan Strait location, almost 20% of the WECs are above CF 25% while less than 10% of the WECs have CF 13%. Almost half the OWTs in this location have CF equal or higher than 30%. Results for the two case studies validate the optimal results generated by the algorithm and the goodness of fit of the selected areas.

The wave wake preprocessing method can be seamless integrated with other optimization algorithms in addition to GA to evaluate layouts of combined wave-wind farms. The new layout optimization method was designed with a plug in approach, which allows different wave energy converters or wind turbine models, diverse wake (wave or wind) models, new meteorological data or alternative geographical information to be easily applied to the method without major modifications on the method itself. Therefore, other energy devices with diverse safety distance specification will be explore to evaluate the performance of the

methodology on diverse meteorological conditions and geographical locations. In addition, the preprocessing concept for calculating wave wakes can be used with other optimization methods without major changes on the calculation processes, such as particle swarm optimization, ant colony optimization, etc. Furthermore, the wave and wind wake models can be analyzed and validated applying high resolution satellite remote sensing to evaluate its fitness for the optimization method. If required, wake models could be further calibrated to adjust to real conditions reported by remote sensing (or other systems) and create more accurate models. It is also important to point out that the approaches to apply safety distance and restricted area rules should be tested when the studying locations change due to the change of wind and wave conditions. Furthermore, as OWTs grow in size and NPC the number of wind harvesters compared with WECs may be recalibrated and safety distances adjusted to optimize total energy extraction at each location. At last, the variations on other factors, such as air density and salinity, can be considered in the power output calculation process if the changes are too big to be neglected.

Credit authorship contribution statement

Francisco Haces-Fernandez: Methodology, Software, Data curation, Formal analysis, Writing - original draft. **Hua Li:** Conceptualization, Methodology, Supervision. **David Ramirez:** Supervision.

Declaration of Competing Interest

The authors declare that they have no known competing financial interests or personal relationships that could have appeared to influence the work reported in this paper.

Acknowledgements

The authors are thankful to the support from CONACYT (Consejo Nacional de Ciencia y Tecnología) and COTACYT (Consejo Tamaulipeco de Ciencia y Tecnologia) through the scholarship number 218681, Planet Labs Education and Research Program for the access to its datasets and remote sensing data for our research project, U.S. Geological Survey and NASA for satellite remote sense images, Texas A&M University-Kingsville, Eagle Ford Center for Research and Outreach, the Center for Research Excellence in Science and Technology - Research on Environmental Sustainability in Semi-Arid Coastal Areas (CREST-RESSACA) and National Science Foundation (award # EEC 1757812).

References

[1] Cruz J, 2007, Ocean wave energy: Current status and future prespectives. Springer Science & Business Media.
[2] Lewis A, Estefen S, Huckerby J, Musial W, Pontes TJ, Torres-Martinez, 2011, Ocean Energy. In IPCC Special Report on Renewable Energy Sources and Climate Change Mitigation. Cambridge University Press, Cambridge, United Kingdom and New York, NY, USA.
[3] Tibbetts J. Coastal cities: Living on the edge. Environ Health Perspect 2002;110 (11):A674.
[4] Sawin JL, Sverrisson F, Seyboth K, Adib R, Murdock HE, Lins C, Jawahar R, 2016, Renewables 2016 Global Status Report. Key findings. A Record Breaking Year for Renewable Energy: New Installations, Policy Targets, Investment and Jobs. Mainstreaming renewables: guidance for policy makers.
[5] Electric Power Research Institute -EPRI (2011) Mapping and Assessment of the United States Ocean Wave Energy Resource, 2011. Technical Report.
[6] Lehmann Marcus, Karimpour Farid, Goudey Clifford A, Jacobson Paul T, Alam Mohammad-Reza. Ocean wave energy in the United States: Current status and future perspectives. Renew Sustain Energy Rev 2017;74:1300–13.
[7] Haces-Fernandez F, Li H, Ramirez D. Assessment of the potential of energy extracted from waves and wind to supply offshore oil platforms operating in the Gulf of Mexico. Energies 2018;11(5):1084.
[8] Zheng ChongWei, Zhuang Hui, Li Xin, Li XunQiang. Wind energy and wave energy resources assessment in the East China Sea and South China Sea. Sci China Technol Sci 2012;55(1):163–73.
[9] Aderinto T, Li H. Ocean wave energy converters: Status and challenges. Energies 2018;11(5):1250.
[10] Levitan D, 2014, Why Wave Power Has Lagged Far behind as Energy Source. Yale Environment 360, retrieved February 20th, 2015, http://e360. yale. edu-/feature /why_wave_power_has_lagged_far_behind_as_energy_source/2760.
[11] Cornett AM, 2008, January. A global wave energy resource assessment. In The Eighteenth International Offshore and Polar Engineering Conference. International Society of Offshore and Polar Engineers.
[12] Haces-Fernandez Francisco, Li Hua, Ramirez David. Wave energy characterization and assessment in the US Gulf of Mexico, East and West Coasts with Energy Event concept. Renew Energy 2018;123:312–22.
[13] Astariz S, Iglesias G. The economics of wave energy: A review. Renew Sustain Energy Rev 2015;45:397–408.
[14] Musial WD, 2008, Status of wave and tidal power technologies for the United States. Golden: National Renewable Energy Laboratory.
[15] Blummarch PA, 2009, Setback for Wave Power Technology, New York Times published on March 16, 2009, http://www.nytimes.com/2009/03/16/ business/global/16iht-renport.html. Last consulted June 14, 2017.
[16] Coe RG, Neary VS. Review of methods for modeling wave energy converter survival in extreme sea states. Proceedings of the 2nd Marine Energy Technology Symposium. METS2014. 2014.
[17] Tiron Roxana, Mallon Fionn, Dias Frédéric, Reynaud Emmanuel G. The challenging life of wave energy devices at sea: A few points to consider. Renew Sustain Energy Rev 2015;43:1263–72.
[18] Meekins R, Adams S, Farinholt K, Hipwell N, Desrosiers M, Beling P, 2017, Impact damage prediction for wave energy converters. In Annual Conference of the Prognostics and Health Management Society 2017.
[19] Falnes Johannes. A review of wave-energy extraction. Mar struct 2007;20(4): 185–201.
[20] Bozzi S, Archetti R, Passoni G. Wave electricity production in Italian offshore: A preliminary investigation. Renew Energy 2014;62:407–16.
[21] Rusu E. Evaluation of the wave energy conversion efficiency in various coastal environments. Energies 2014;7(6):4002–18.
[22] Stoutenburg Eric D, Jenkins Nicholas, Jacobson Mark Z. Power output variations of co-located offshore wind turbines and wave energy converters in California. Renew Energy 2010;35(12):2781–91.
[23] Haces-Fernandez F, Li H, Jin K. Investigation on the possibility of extracting wave energy from the Texas coast. Int J Energy Clean Environ 2018.
[24] Rusu E, Onea F. A review of the technologies for wave energy extraction. Clean Energy 2018;2(1):10–9.
[25] Clemente D, Rosa-Santos P, Taveira-Pinto F. On the potential synergies and applications of wave energy converters: A review. Renew Sustain Energy Rev 2021; 135:110162. https://doi.org/10.1016/j.rser.2020.110162.
[26] Fusco Francesco, Nolan Gary, Ringwood John V. Variability reduction through optimal combination of wind/wave resources-An Irish case study. Energy 2010;35 (1):314–25.
[27] Widén Joakim, Carpman Nicole, Castellucci Valeria, Lingfors David, Olauson Jon, Remouit Flore, et al. Variability assessment and forecasting of renewables: A review for solar, wind, wave and tidal resources. Renew Sustain Energy Rev 2015; 44:356–75.
[28] Izquierdo-Pérez J, Brentan BM, Izquierdo J, Clausen NE, Pegalajar-Jurado A, Ebsen N. Layout optimization process to minimize the cost of energy of an offshore floating hybrid wind–wave farm. Processes 2020;8(2):139.
[29] Darmon A, Benzaquen M, Raphaël E, 2013, A solution to the Kelvin wake angle controversy. J Fluid Mech, 73(arXiv: 1309.6751), 8.
[30] He Jiayi, Zhang Chenliang, Zhu Yi, Wu Huiyu, Yang Chen-Jun, Noblesse Francis, et al. Comparison of three simple models of Kelvin's ship wake. Eur. J. Mech. B Fluids 2015;49:12–9.
[31] Noblesse Francis, Zhang Chenliang, He Jiayi, Zhu Yi, Yang Chenjun, Li Wei. Observations and computations of narrow Kelvin ship wakes. J Ocean Eng Sci 2016;1(1):52–65.
[32] Kim JW, Magee A, Guan KYH. In: CFD simulation of flow-induced motions of a multi-column floating platform. American Society of Mechanical Engineers; 2011. p. 319–26.
[33] Rusu Eugen, Guedes Soares C. Coastal impact induced by a Pelamis wave farm operating in the Portuguese nearshore. Renew Energy 2013;58:34–49.
[34] Folley M, Babarit A, Child B, Forehand D, O'Boyle L, Silverthorne K, et al. In: A review of numerical modelling of wave energy converter arrays. American Society of Mechanical Engineers; 2012. p. 535–45.
[35] Wang Ben-long, Guo Xiao-yu, Liu Hua, He Chen. Numerical simulations of wake signatures around high-speed ships. J Hydrodyn Ser B 2014;26(6):986–9.
[36] Crawford FS. Elementary derivation of the wake pattern of a boat. Am J Phys 1984; 52(9):782–5.
[37] Bai L, Spence RR, Dudziak G. Investigation of the influence of array arrangement and spacing on tidal energy converter (TEC) performance using a 3-dimensional CFD model. In: Proceedings of the 8th European wave and tidal energy conference; 2009. p. 654–60.
[38] Peltzer R, Garrett W, Smith P. A remote sensing study of a surface ship wake. In: OCEANS'85-Ocean Engineering and the Environment. IEEE; 1985. p. 277–86.
[39] Penney WG, Price AT. Part I. The diffraction theory of sea waves and the shelter afforded by breakwaters. Philos Trans R Soc Lond A 1952;244(882):236–53.
[40] Hotta S, 1980, Wave height distribution around permeable breakwaters. In Coastal Engineering 1980 (pp. 221–240).
[41] Monk Kieran, Zou Qingping, Conley Daniel. An approximate solution for the wave energy shadow in the lee of an array of overtopping type wave energy converters. Coast Eng 2013;73:115–32.

[42] Kim Hanna, Do Ki Deok, Suh Kyung-Duck. Scattering of obliquely incident water waves by partially reflecting non-transmitting breakwaters. Ocean Eng 2011;38(1):148–58.
[43] Babarit A. A database of capture width ratio of wave energy converters. Renew Energy 2015;80:610–28.
[44] Thiam AG, Pierce AD, 2010, November, Segmented and continuous beam models for the capture of ocean wave energy by Pelamis-like devices. Proceedings of Meetings on Acoustics 160ASA, Vol. 11, No. 1, p. 065001. ASA.
[45] Rainey RCT. The Pelamis wave energy converter: it may be jolly good in practice, but will it work in theory. Proc. 16th Int'l. Workshop on Water Waves and Floating Bodies. 2001.
[46] Kim SD, Lee HJ. The comparison of analytical and numerical solutions for wave diffraction due to insular breakwater. Int J Phys Sci 2010;5(3):226–37.
[47] Ou SH, Tzang SY, Hsu TW, 1989, Wave field behind the permeable detached breakwater. In Coastal Engineering 1988, p. 121–135.
[48] McCormick Michael E, Kraemer David RB. Polynomial approximations for Fresnel integrals in diffraction analysis. Coast Eng 2002;44(3):261–6.
[49] Tomey-Bozo Nicolas, Murphy Jimmy, Troch Peter, Lewis Tony, Thomas Gareth. Modelling of a flap-type wave energy converter farm in a mild-slope equation model for a wake effect assessment. IET Renew Power Gener 2017;11(9):1142–52.
[50] Jensen NO, 1983. A note on wind generator interaction.
[51] Frandsen Sten. On the wind speed reduction in the center of large clusters of wind turbines. J Wind Eng Ind Aerodyn 1992;39(1-3):251–65.
[52] Katic I, Højstrup J, Jensen NO. A simple model for cluster efficiency. In: European wind energy association conference and exhibition; 1986. p. 407–10.
[53] Sorensen P, Nielsen T. Recalibrating wind turbine wake model parameters-validating the wake model performance for large offshore wind farms. European Wind Energy Conference and Exhibition. 2006.
[54] Mosetti G, Poloni C, Diviacco B. Optimization of wind turbine positioning in large windfarms by means of a genetic algorithm. J Wind Eng Ind Aerodyn 1994;51(1):105–16.
[55] Chen Y, Li H, Jin K, Song Q. Wind farm layout optimization using genetic algorithm with different hub height wind turbines. Energy Convers Manage 2013;70:56–65.
[56] Shakoor Rabia, Hassan Mohammad Yusri, Raheem Abdur, Wu Yuan-Kang. Wake effect modeling: A review of wind farm layout optimization using Jensen's model. Renew Sustain Energy Rev 2016;58:1048–59.
[57] Beltau A, 2016a, Calculation: 10MW (8MW) alternatief: Kavel IV. Vestas V164-8.0-8.000. Project: 715082. Pondera Consult B.V. Published by the Commission for the Environmental Impact Assessment of the Netherlands. https://www.commissiemer.nl/projectdocumenten/ 00002269.pdf? documenttitle=Bijlage%2012.2%20-%20WindPRO%20-%20PARK_% 2010MW%20 (8MW)%20alterna2.pdf. Last consulted July 27, 2020.
[58] Beltau A, 2016b, Calculation: 6MW alternatief: Kavel IV. alternatief: Kavel IV. Siemens SWT-6.0-154-6.000. Project: 715082. Pondera Consult B.V. Published by the Commission for the Environmental Impact Assessment of the Netherlands. https://www.commissiemer.nl/projectdocumenten/00002268.pdf?documenttitle=Bijlage%2012.1%20-%20WindPRO%20-%20PARK_%206MW%20alternatief_%20K2.pdf, Last consulted July 27, 2018.
[59] González Javier Serrano, Gonzalez Rodriguez Angel G, Mora José Castro, Santos Jesús Riquelme, Payan Manuel Burgos. Optimization of wind farm turbines layout using an evolutive algorithm. Renew Energy 2010;35(8):1671–81.
[60] Grady SA, Hussaini MY, Abdullah MM. Placement of wind turbines using genetic algorithms. Renew Energy 2005;30(2):259–70.
[61] Bahaj AS. Generating electricity from the oceans. Renew Sustain Energy Rev 2011;15(7):3399–416.
[62] EMEC, 2018, Pelamis Wave Power. EMEC. The European Marine Energy Center LTD. Orkney, Scotland. Available online: http://www.emec.org.uk/about-us/wave-clients/pelamis-wave-power/ (accessed on 25 October 2018).
[63] Wan Yong, Fan Chenqing, Dai Yongshou, Li Ligang, Sun Weifeng, Zhou Peng, et al. Assessment of the joint development potential of wave and wind energy in the South China Sea. Energies 2018;11(2):398. https://doi.org/10.3390/en11020398.
[64] Chadee XT, Clarke RM, 2013. Air density climate of two caribbean tropical islands and relevance to wind power. International Scholarly Research Notices, 2013.
[65] IRENA, 2016, Floating Foundations: A Game Changer for Offshore Wind Power, International. Renewable Energy Agency, Abu Dhabi. 2016. Available online: http://www.irena.org/-/media/Files/IRENA/Agency/Publication/2016/IRENA_Offshore_Wind_Floating_Foundations_2016.pdf (accessed on 25 October 2018).
[66] EWEA. European Wind Energy Association, 2013, Deep Water: The Next Step for Offshore Wind Energy. July 2013 Available online: https://windeurope.org/about-wind/reports/deep-water/ (accessed on 16 Apr 2021).
[67] U.S. Department of Energy, 2017, Wind on the Waves: Floating Wind Power Is Becoming a Reality; Office of Energy Efficiency and Renewable Energy U.S. Department of Energy: Washington, DC, USA, 2017.
[68] Haces-Fernandez F, 2014, Investigation on the Possibility of Extracting Wave Energy from the Texas Coast. ProQuest Dissertations and Theses; Thesis (M.S.) Texas A&M University - Kingsville, 2014; Publication Number: AAT 1572637; ISBN: 9781321473230;.
[69] Juan Angel A, Faulin Javier, Grasman Scott E, Rabe Markus, Figueira Gonçalo. A review of simheuristics: Extending metaheuristics to deal with stochastic combinatorial optimization problems. Oper Res Perspect 2015;2:62–72.
[70] Evans PR. Rotations and rotation matrices. Acta Crystallogr D Biol Crystallogr 2001;57(10):1355–9.
[71] Spindler DM, Chawla A, Tolman HL, 2011, An initial look at the CFSR Reanalysis winds for wave modeling. Technical Note, MMAB Contribution, (290).
[72] Feng Y, Tavner PJ, Long H. Early experiences with UK Round 1 offshore wind farms. Proc Inst Civ Eng Energy 2010;163(4):167–81.
[73] Wiser R, Bolinger M, Barbose G, Darghouth N, Hoen B, Mills A, Widiss R, 2015, Wind Technologies Market Report; U.S. Department of Energy (DOE): Washington, DC, USA, 2015.